Pergamon

Int. J. Heat Mass Transfer. Vol. 40, No. 8, pp. 1773–1793, 1997

0017–9310/97 $17.00 + 0.00

PII: S0017–9310(96)00254–2

A 3-D Eulerian–Lagrangian model of dispersed flow film boiling—II. Assessment using quasi-steady-state data and comparison with the results of 1-D analyses

M. ANDREANI and G. YADIGAROGLU

Nuclear Engineering Laboratory, Swiss Federal Institute of Technology, ETH, ETH-Zentrum, CLT, CH-8092 Zurich, Switzerland

(*Received* 16 *July* 1996)

Abstract—The hybrid Eulerian–Lagrangian model developed in the companion paper (Part I) is assessed against several post-critical-heat-flux data sets, obtained in both reflooding and slowly advancing quench front experiments using the hot patch technique. The calculated results are generally in good agreement with the data; the good prediction of the high vapour superheats is due to the low values of the interfacial heat transfer which results from the droplet clustering around the centre of the channel. For comparison with the usual one-dimensional approaches, a one-dimensional model is also derived, which uses a single diameter representing the droplet population, and its results are compared with those obtained by the new three-dimensional model. For conditions of low mass flux and not very high void fraction at the quench front, the 1-D analyses underpredict the vapour superheat as the calculated interfacial heat transfers are presumedly too high. The limitations of the models implemented in the large reactor safety computer codes are also discussed. © 1997 Elsevier Science Ltd. All rights reserved.

1. INTRODUCTION

A new hybrid Eulerian–Lagrangian model for dispersed flow film boiling has been developed in a companion paper (Part I [1]), which couples a two-dimensional Eulerian calculation of the vapour field with a three-dimensional Lagrangian description of the droplet hydrodynamics.

The model is intended for quasi-steady conditions above the quench front in a tube; positive quality at the quench front and annular flow regime immediately below are assumed. The experimental heat flux is provided as a boundary condition and the results include radial and axial profiles of void fraction and temperature of the vapour phase and all the main quantities (sizes, velocities and their distributions) characterizing the droplet population.

Full assessment of the model would, thus, require comparison of all these variables with experimental values. Unfortunately, the only measured values which are available from tube experiments are the axial profiles of the wall temperature and the average vapour temperature at some locations. In a few cases, the average void fraction at certain locations and the droplet size distribution at the tube exit have also been measured.

Since the main reason for developing a new model was to overcome the limitations of the current calculation methods [2], with respect to droplet hydrodynamics and their interactions with the vapour field, the most interesting variable for evaluation of the model is the vapour temperature.†

2. DATA SETS USED FOR THE ASSESSMENT

Owing to the special importance of the vapour temperature for the verification of the model, only recent data sets including such measurements are considered here, Table 1. Experimental results including only wall temperatures have, however, also been used when (atmospheric pressure, low mass flux conditions) more complete data have not been found in the literature.

UC-B Experiments

Two series of reflooding experiments were carried-out at the University of California at Berkeley in a tube 3.67 m in height: the first series, at atmospheric pressure [4] with a tube of 14.4 mm in internal diameter, and a second series at 2 and 3 bar [5] with a 14.25 mm tube. The tubes were not insulated. During many

† In the following, it will be assumed that the *experimental* vapour temperatures are bulk values; consistently, the *calculated* vapour temperatures will be obtained from the radial temperature distribution (output of the model) by calculating the cross-sectional average of the product of the local axial vapour velocity and temperature. The difficulties associated with the comparison between calculated and measured vapour temperatures are discussed by Andreani [3]. In general, it can be argued that the experimental value is a lower bound for the actual bulk temperature.

NOMENCLATURE

A	flow area of the tube [m^2]
d	droplet diameter [m]
d_{32}	Sauter mean diameter (*SMD*) [m]
d_{50}	volume median diameter [m]
D	internal tube diameter [m]
G	mass flux [kg m^{-2} s^{-1}]
h	heat transfer coefficient [W m^{-2} K^{-1}]
k_r	droplet initial radial velocity multiplier
$\dot{M}$	mass flow rate [kg s^{-1}]
p	pressure [bar]
q''	heat flux [W m^{-2}]
q''_c	convective heat flux [W m^{-2}]
q''_{dc}	direct-contact wall-to-droplet heat flux [W m^{-2}]
q''_{qf}	radiative heat flux vapour-to-liquid [W m^{-2}]
q''_i	interfacial heat transfer rate per unit wall area [W m^{-2}]
$q''_{i,1\text{-}D}$	equivalent 1-D interfacial heat flux [W m^{-2}]
q''_{rad}	radiative heat flux from the wall $= q''_{wf}+q''_{wg}$ [W m^{-2}]
q''_{wf}	wall-to-liquid radiative heat flux [W m^{-2}]
q''_{wg}	wall-to-vapour radiative heat flux [W m^{-2}]
$q''_{gi}, -Q_{ig}$	Interfacial heat transfer rate per unit volume [W m^{-3}]
r	radial coordinate, distance from the tube axis [m]
SMD	Sauter mean diameter, d_{32} [m]
t	time [s]
T	temperature [°C or K]
U	cross-sectional average vapour velocity [m s^{-1}]
x	quality
w	droplet velocity [m s^{-1}]
W_z	average axial liquid velocity [m s^{-1}]
We	Weber number $= \rho_g U_{fg}^2 d/\sigma$
z	axial coordinate [m].

Greek symbols

α_g	void fraction
Γ	volumetric vapour generation rate [kg m^{-3} s^{-1}]
μ	dynamic viscosity [kg m^{-1} s^{-1}]
ρ	density [kg m^{-3}]
σ	surface tension [kg s^{-2}]
ϕ	angle.

Subscripts

eq	equilibrium (for droplet population)
E	thermal equilibrium
f	liquid
g	vapour
fg	difference between the two phases
i	interface
m	maximum
r	in radial direction
s	saturation rate
w	wall or wave
z	in axial direction
0	at the quench front location.

Superscripts

*	in the reference calculation
T	at the tube exit
+	above quench front
−	below quench front.

tests, the wall temperature at some distance from the quench front reached practically a steady condition, where the heat input was balanced by the losses and heat transfer to the fluid. This condition is the most favourable for analysis by a steady-state model; the axial distribution of wall temperature and the exit vapour temperature (when available) after this 'plateau' is reached, can be used for assessment. Under such conditions the quality at the quench front was usually positive, indicating the presence of dispersed flow. The instantaneous measurements at the earliest time at which this steady condition was reached are chosen for the assessment. For three runs, the experimental conditions at later times are also considered. These data points are identified by the elevation (in feet) of the quench front: for example Test U137$_3$ means that the experimental wall and vapour temperatures are selected at the time the quench front was (approximately) 0.91 m (3 ft) above the bottom of the heated section of Run 137. Some of the runs lack information on the vapour temperature (the thermocouple measuring the exit vapour temperature had quenched), but some of these tests were included in the assessment matrix because, as it will be made evident later, the test conditions (low mass flux) of these runs deserve special attention.

For three tests, U126, U137$_6$ and U194$_6$, an estimation of the droplet size distribution and characteristic mean diameters at the tube exit are available [8]. In spite of shortcomings of the statistics, important information is obtained from the visual observations: dimension of the largest stable droplet, relative abundance of small and large diameters, *possible* presence of significant break-up phenomena in a large

Table 1. Experimental conditions used for the assessment

Test section	Run no.	z_{QF} (m)	p (bar)	G (kg m^{-2} s^{-1})	x^-	U_{QF} (mm s^{-1})	z^T (m)	x_E^T	Test identification
UC-B [4]	118	1.01	1.0	24.0	0.09	2.2	3.65	0.25	U118
	122	1.37	1.0	24.3	0.10	1.6		0.23	U122
	126	1.83	1.0	73.0	0.03	3.0		0.08	U126
	136	1.83	1.0	125.0	0.03	3.0		0.08	U136
	137	1.13	1.0	75.0	0.03	2.7		0.13	$U137_3$
		1.37	1.0	75.0	0.05	2.7		0.14	$U137_4$
		1.83	1.0	75.0	0.09	2.8		0.17	$U137_6$
	180	0.99	1.0	24.8	0.10	2.1		0.24	$U180_3$
		1.37	1.0	24.8	0.16	1.7		0.28	$U180_4$
		1.83	1.0	24.8	0.24	1.7		0.36	$U180_6$
	194	1.83	1.0	75.0	0.01	5.2		0.10	$U194_6$
		2.07	1.0	75.0	0.04	2.5		0.11	$U194_7$
UC-B [5]	3051	1.90	2.0	25.1	0.09	7.3	3.65	0.22	U351
	3053	2.05	3.0	25.0	0.11	7.5		0.25	U353
	3058	1.83	2.0	75.4	0.03	4.1		0.13	U358
	3059	1.83	3.0	75.1	0.04	5.8		0.16	U359
Lehigh	100(1)	0.12	3.8	14.8	0.62		1.31	0.89	L100
University [6]	103(1)	0.29	5.4	28.8	0.39			0.58	L103
	106(1)	0.29	2.5	15.2	0.26			0.46	L106
	109(1)	0.19	2.4	15.2	0.36			0.55	L109
	111(1)	0.19	3.9	14.8	0.75			1.05	L111
	112(1)	0.30	4.1	20.7	0.54			0.77	L112
	114(1)	0.20	4.1	21.0	0.15			0.41	L114
	115(1)	0.19	4.1	21.0	0.25			0.49	L115
	118(1)	0.19	2.6	14.9	0.44			0.67	L118
	124(1)	0.32	4.0	42.7	0.39			0.54	L124
	129(2)	0.30	5.3	14.8	0.06			0.54	L129
	140(3)	0.31	5.3	74.0	0.19			0.32	L140
	153(4)	0.30	2.7	76.5	0.18			0.25	L153
	154(4)	0.30	2.5	77.3	0.09			0.14	L154
INEL [7]	113	0.11	3.7	43.1	0.42		1.84	0.66	I113
	222	0.25	7.0	75.1	0.23		1.23	0.43	I222

Regarding the Lehigh University Tests [6], the numbers in parentheses in the second column refer to the run rating: the most accurate measurements were obtained for rating 1 runs.

portion of the heated length, etc. This information is valuable for the assessment of the break-up model used here.

Lehigh University Tests

These experiments [6] were performed with an insulated tube (1.35 m in length and with an internal diameter of 15.4 mm) at pressures up to 5 atm. Slowly-moving quench front experiments were mostly run, due to the experimental difficulty of maintaining a fixed critical-heat-flux point under a wide range of operational conditions. The data points selected for the assessment were the first measurements (lowest elevation of the quench front—the model is best tested if the calculation can extend over a sufficiently long section) of tests having the best rating [6]. Some lower rating experiments had also to be analysed to extend the range of the assessment: in fact, no intermediate mass flux test got the highest rating.

INEL Tests

Similar experiments conducted at the Idaho National Engineering Laboratory [7] provided non-equilibrium data at pressures up to 70 bar. The test section consisted of a vertical, Inconel-625 insulated tube, with 15.7 mm internal diameter; the heated length was 2.134 m. Wall temperatures were measured at 38 axial elevations. The vapour temperature was measured by steam probes at three elevations, but for many experiments only one or two temperatures are given. Two runs at intermediate mass flux have been used from this set, as few data for pressures higher than 1 bar could be obtained from the other data sets.

The experimental results used for the assessment cover the following range of variables:

$1 <$ pressure, $p < 7$ bar
$15 <$ mass flux, $G < 125$ kg m^{-2} s^{-1}
$0.02 <$ quality at the quench front, $x^- < 0.8$

The experimental conditions for the 32 tests analyzed are summarized in Table 1.

3. INITIAL CONDITIONS

The flow conditions at the quench front elevation, calculated using the methods outlined in the com-

Table 2. Calculated initial conditions at the quench front

Test no.	x^+	$\langle\alpha_g\rangle$	$W_{z,0}$ (m s^{-1})	$U_{z,0}$	Re_g ($\times 10^{-3}$)	$w_{r,A}$ (m s^{-1})	k_r^*	$w_{r,m}$ (m s^{-1})	SMD_0 (mm)	$d_{m,0}$ (mm)	$We_{m,0}$
U118	0.11	0.966	0.7	4.4	3.1	0.09	3.6	0.32	7.0	13.3	2.1
U122	0.11	0.967	0.7	4.5	3.5	0.09	3.6	0.32	6.9	13.3	2.1
U126	0.04	0.946	1.4	4.8	3.5	0.10	5.2	0.50	8.5	13.3	1.8
U136	0.03	0.949	2.5	6.7	4.8	0.13	4.2	0.54	8.5	13.3	2.6
$U137_3$	0.04	0.945	1.4	4.7	3.4	0.10	5.2	0.50	8.5	13.3	1.8
$U137_4$	0.06	0.962	2.0	7.3	5.1	0.14	3.9	0.54	7.4	13.3	4.0
$U137_6$	0.09	0.978	3.1	12.3	8.7	0.22	1.7	0.38	5.3	13.3	11.7
$U180_3$	0.11	0.967	0.7	4.7	3.3	0.09	3.4	0.32	6.8	13.3	2.2
$U180_4$	0.17	0.977	0.9	7.4	5.2	0.14	1.1	0.15	5.0	13.3	5.9
$U180_6$	0.25	0.983	1.1	10.7	7.5	0.19	0.0	0.0	3.9	11.3	10.7
$U194_6$	0.02	0.903	0.8	3.2	2.3	0.07	5.2	0.35	8.4	13.3	0.9
$U194_7$	0.04	0.955	1.6	6.0	4.2	0.11	4.7	0.54	8.1	13.3	2.7
U351	0.12	0.951	0.5	2.7	3.5	0.08	3.7	0.28	3.1	9.2	1.0
U353	0.14	0.947	0.4	2.2	4.0	0.07	4.7	0.35	3.1	9.2	1.0
U358	0.04	0.916	0.9	3.1	4.0	0.09	6.6	0.56	8.4	13.3	1.5
U359	0.06	0.909	0.8	2.7	5.0	0.09	6.4	0.56	8.4	13.3	1.6
L100	0.64	0.985	0.4	4.6	11.0	0.15	3.1	0.46	3.0	8.5	6.4
L103	0.43	0.969	0.6	4.3	14.1	0.16	5.0	0.83	4.0	11.5	10.3
L106	0.31	0.972	0.4	3.4	5.7	0.10	0.0	0.0	5.2	14.3	3.6
L109	0.38	0.978	0.4	4.3	7.0	0.12	0.0	0.0	4.4	13.1	5.1
L111	0.80	0.991	0.3	5.5	13.6	0.18	3.9	0.69	2.2	6.3	7.3
L112	0.59	0.981	0.5	5.5	14.1	0.18	3.6	0.66	3.0	9.0	10.5
L114	0.21	0.949	0.4	2.1	5.3	0.08	8.2	0.64	5.1	14.3	2.0
L115	0.30	0.962	0.4	2.9	7.4	0.10	3.7	0.38	5.4	14.3	4.1
L118	0.48	0.981	0.4	4.9	8.6	0.14	0.0	0.0	3.6	10.5	6.1
L124	0.42	0.977	1.1	8.3	20.9	0.26	1.5	0.39	3.3	10.6	22.0
L129	0.21	0.830	0.1	1.3	4.2	0.06	12.1	0.70	1.6	4.4	0.4
L140	0.22	0.957	1.4	5.9	18.9	0.21	3.6	0.78	4.9	14.3	17.9
L153	0.19	0.972	2.4	9.7	17.5	0.25	0.3	0.07	4.6	13.4	21.2
L154	0.10	0.951	1.5	5.7	9.6	0.15	2.8	0.42	6.8	14.3	6.8
I113	0.42	0.979	1.2	9.0	21.1	0.26	0.9	0.23	3.2	9.3	23.1
I222	0.25	0.954	1.3	5.1	19.7	0.20	3.2	0.65	4.9	14.3	15.9

panion paper [1] are listed in Table 2. The maximum initial radial velocity of the droplets $w_{r,m}$ is obtained by multiplying the value obtained in annular flow experiments $w_{r,A}$ by a multiplier k_r, different for each test. The value of k_r which allows the best prediction of the experimental temperature is denoted by k_r^*.

It has been found that k_r^* follows a certain trend: it decreases for increasing mass flux and quality, and increases with pressure. No attempt was made to find any theoretical foundation for this result, as a detailed model for drop formation would have been required to produce theoretical values for k_r: no related data, however, are available to date and any theoretical speculation would have been on uncertain ground. In this respect k_r^* has to be regarded as a (consistently varying) best-fit parameter, and the role played by such a 'tuning' factor will become clear in the following sections. No *simple* relation has been found that correlates k_r^* with quality, mass flux and pressure. For any predictive purpose, k_r^* could be obtained by interpolation (inside the range of conditions investigated here) of the best-fit values presented in Table 2. The calculations carried out with $k_r = k_r^*$ from now on will be referred to as 'reference' calculations.

4. REFERENCE CALCULATIONS

The only adjustable parameter in the model is the radial velocity multiplier k_r; calculations have been carried out for all the tests for the reference value k_r^*, as well as for k_r^*+1 and k_r^*-1. This parametric study allows to evaluate the influence of this parameter and to justify the choice of the reference value.

4.1. *Representative results of the 3-D model*

As mentioned above, full assessment of the model can be accomplished only against data sets including information on the droplet volume distribution and related mean diameters. In this respect the three tests U126, $U137_6$, and $U194_6$, all at atmospheric pressure, have a special importance, as they are the only ones that provide droplet spectrum data, at least at the tube exit. The comparison of calculated and experimental results starts, therefore, with a detailed discussion of one of these cases, namely test $U137_6$. The complete analyses of the results for all three tests are reported by Andreani [3].

Test U137 was run under intermediate flooding rate

(7.5 cm s^{-1}) and high heat flux conditions. The quality above the quench front at the time of the half-length quench was ≈ 0.1, so that the void fraction must have been larger than 95%: dispersed flow certainly prevailed above the quench front.

4.1.1. *Wall temperatures and cross-sectional average variables.* Figure 1 shows the axial evolution of the calculated wall and vapour temperatures, together with the experimental wall temperatures at different elevations and the vapour temperature at the tube exit.† The agreement between calculated and measured wall temperatures and vapour exit temperatures is rather good for all k_r values. The only discernible deficiency of the model (for k_r^* and k_r^*-1) concerns the prediction of the wall temperatures in the near-quench front region (up to 70 cm), where the wall temperature is overpredicted. Increasing k_r allows a much better prediction near the quench front, and still a good prediction far from it.

Far from the quench front, the calculation shows a moderate sensitivity to k_r: wall temperatures remain in a band of 50 K. To explain the lack of sensitivity of the calculations in this region to k_r, the relative magnitude of the various heat fluxes must be presented first (Fig. 2). In order to compare directly the heat inputs from the wall to the vapour (due to convection, q_c'' and radiation, q_{wg}'') with the heat sink (i.e. the interfacial heat transfer to the droplets) an interfacial heat

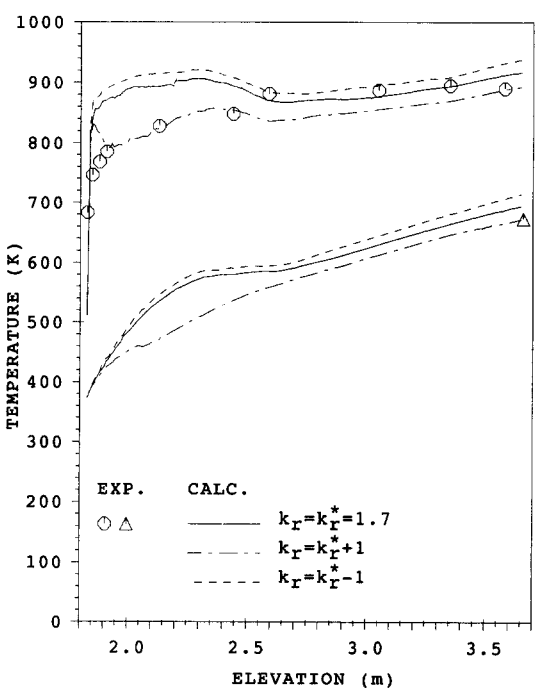

Fig. 1. Comparison of measured and calculated wall and vapour temperatures for test U137$_6$ ($p = 1$ bar; $G = 75$ kg m^{-2} s^{-1}, $x^+ = 0.09$), for three values of k_r.

† In this and in the following figures a ○ denotes experimental wall temperatures and a △ experimental vapour temperatures. The upper family of curves represents (obviously) the calculated wall temperatures.

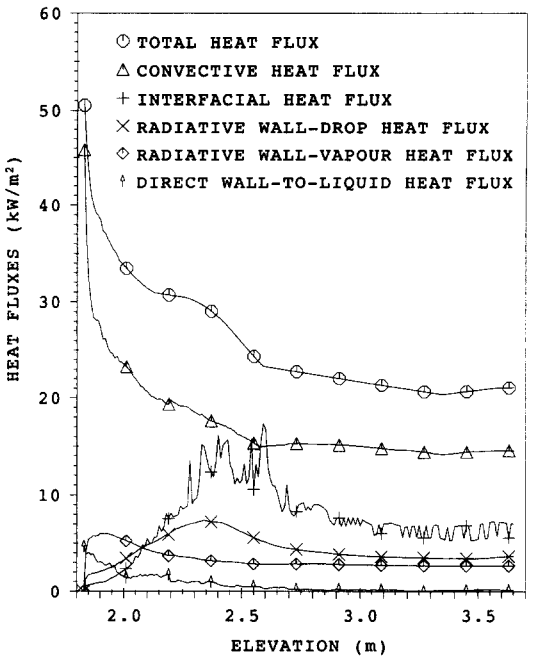

Fig. 2. Calculated heat fluxes for test U137$_6$ (reference calculation).

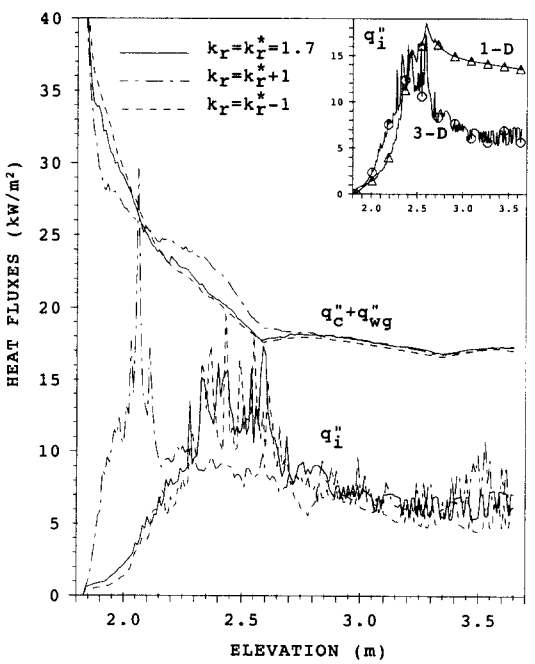

Fig. 3. Calculated total heat flux from the wall to the vapour $q_c''+q_{wg}''$ and interfacial heat flux q_i'' for test U137$_6$.

flux q_i'' is defined as the interfacial heat transfer rate *per unit wall area*:

$$q_i'' = \frac{D}{4}\int_A q_{gi}'''\,dA \qquad (1)$$

The comparison of the sum of the convective and radiative heat fluxes to the vapour with the interfacial heat flux (Fig. 3) shows that the large interfacial heat

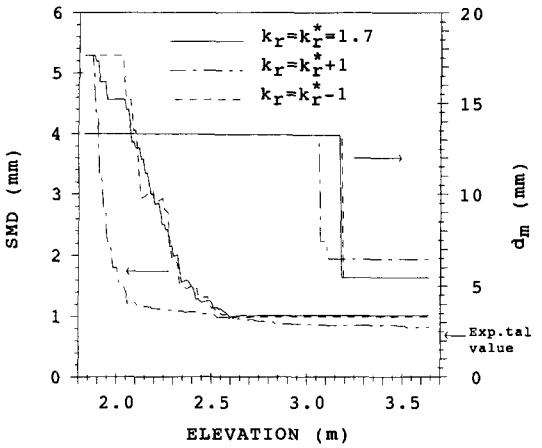

Fig. 4. Axial evolution of the Sauter mean diameter *SMD* and maximum droplet diameter d_m for test U137$_6$.

transfer in the calculation with k_r^*+1 is responsible for the reduced vapour and wall superheats close to the quench front. In this case, further up, q_i'' decreases, while the two runs with k_r^* and k_r^*-1 show a gradual increase of q_i'' up to $z = 2.6$ m. Above this elevation q_i'' is practically the same for the three cases and much lower than $q_c''+q_{wg}''$, so that a continuous vapour temperature increase becomes possible (Figs. 1 and 3).

The droplet Sauter mean diameter histories for the three cases (Fig. 4) and the analysis of the evolution of the number of droplets which have reached the aerodynamic instability condition and of those undergoing break up by impact with the wall [3] explains the differences in the three calculations at short distances from the quench front. In case of high radial velocities ($k_r = k_r^*+1$), many droplets break-up at the wall within a short distance from the quench front, and the Sauter mean diameter drops quickly to a value close to the final one: aerodynamic break-up further reduces the Sauter mean diameter by not more than 20%. The sudden increase of q_i'' is thus due to the large interfacial area created by fragmentation, while the following decrease can be explained only by considering the effects of the liquid radial distribution on the two-dimensional Eulerian field (2-D effects) discussed below (Section 4.1.3). Interfacial heat transfer is controlled by the value of Sauter mean diameter, as the phase velocities and, then, the void fractions are not very different in the three cases [3]. For lower initial radial velocities, only a few droplets break up upon impact on the wall ($k_r = k_r^*$), or none at all ($k_r = k_r^*-1$). In both cases, the equilibrium value of the Sauter mean diameter is dictated by aerodynamic break-up and is reached in a much more gradual way.

The liquid volume vs droplet diameter (in short, volume-diameter) distribution at the tube exit (Fig. 5) also compares well with the observed one;† the diameter ranges in which most of the volume lies are

† The distributions as well as the characteristic diameters have been extracted by the present authors from the raw data presented by Peake [8].

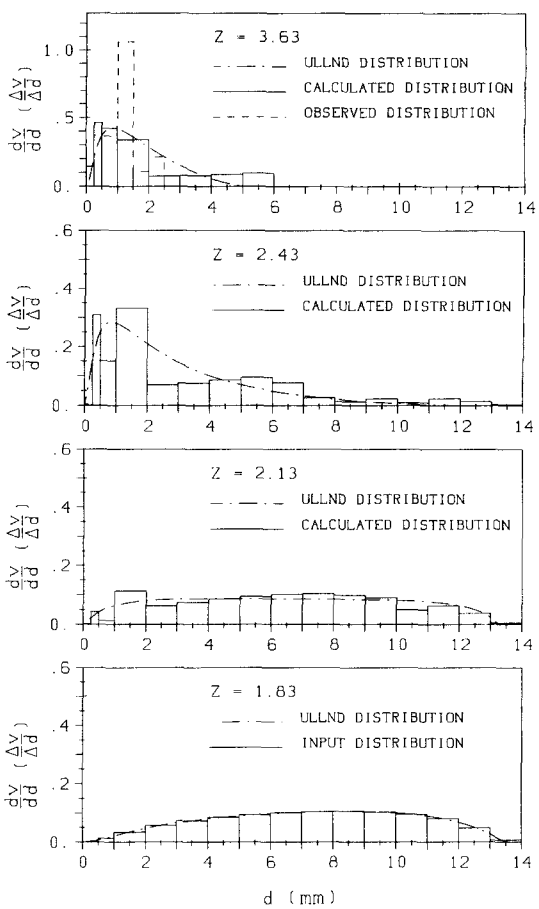

Fig. 5. Axial evolution of the droplet size distribution for test U137$_6$ (reference calculation).

very similar; only the strong peak of the experimental distribution is not predicted. (The only major discrepancy concerns d_m which is larger than the observed one (Figs. 4 and 5); this will be discussed in Section 5.1.) Therefore, regarding the 'equilibrium' droplet distribution reached towards the exit of the tube ($z > 2.6$ m), it can be concluded that the droplet population evolution can be correctly simulated by assuming that aerodynamic break-up is dominating. These arguments favour the aerodynamic break-up as the dominant break-up mechanism in test U137$_6$.

4.1.2. *'Equivalent' 1-D interfacial heat flux.* As reasonable agreement between the calculated and experimental Sauter mean diameters at the tube exit has been obtained for all cases (Figs. 4 and 5), the comparison of the interfacial heat transfer calculated by the present 3-D model with a 1-D calculation using a single diameter is of some interest.

An 'equivalent' 1-D interfacial heat flux (again, referred to the wall), calculated using cross-sectionally averaged quantities is defined as:

$$q''_{i,1\text{-D}} = \frac{4}{D}\frac{6(1-\langle\alpha_g\rangle)}{d_{32}} h_{i,1\text{-D}}(T_b - T_s)$$

$$= \frac{4}{D}\frac{6(1-\langle\alpha_g\rangle)}{d_{32}}\frac{k_g}{d_{32}} Nu_{i,1\text{-D}}(T_b - T_s) \quad (2)$$

where $h_{i,1\text{-D}}$ is the interfacial heat transfer coefficient calculated by the correlation for single droplets (Part I) using average vapour properties and d_{32}. For a given distribution, $h_{i,1\text{-D}}$ and the equivalent interfacial heat transfer should be calculated using d_{20} rather than d_{32} [9], so that $q''_{i,1\text{-D}}$ (calculated with d_{32} d_{32} rather than d_{32} d_{20}) is a lower limit for the 'equivalent' 1-D interfacial heat flux.

From the insert of Fig. 3 one observes that $q''_{i,1\text{-D}}$ is nearly twice as large as q''_i away from the quench front. The equivalent 1-D heat sink would have nearly balanced the heat input to the vapour ($q''_c + q''_{wg}$) downstream from $z = 2.6$ m, and only a very slow increase of the vapour temperature would have been possible, so that it can be inferred that a 1-D calculation may have underpredicted the steam superheat. The lower value of q''_i close to the quench front, on the other hand, leads to an overprediction of the wall temperature.

The 1-D analysis of experiment U137 by Peake [8] showed that large underpredictions of both vapour and wall temperatures were obtained, regardless of the choice of various closure laws and initial conditions. This result is confirmed by Andreani [3]. The limits of the 1-D analyses will be further investigated in Section 6.

Therefore, a first important result can be deduced from the analysis of test U137: only a 3-D calculation allows to predict an interfacial heat transfer that is much lower than that calculated using cross-sectional averages, and this reduction plays a fundamental role in the good prediction of the wall temperatures.

This statement has been systematically checked for all tests in our matrix by calculating the ratio between $q''_{i,1-D}$ and q''_i at the tube exit: the ratio, always larger than one, reached values up to 20.

4.1.3. *2-D effects.* It has been shown that, after the Sauter mean diameter reaches an equilibrium value, the interfacial heat transfer decreases to values that are much lower than those justified by the increase of the void fraction (1-D values) due to the acceleration of the droplets. This reduction can be explained by considering the radial droplet and distributed heat sink distributions.

Figure 6 shows the radial liquid fraction and the non-dimensional temperature profiles at different elevations for test $U137_6$. The curves are plotted for the three different values of k_r. Moreover, the temperature profile obtained by a 1-D calculation (void fraction and heat sink parameter constant over the cross section) performed using the same Sauter mean diameter as that obtained in the reference calculation is included for comparison; more details about these 1-D analyses are given in Section 6. The most striking feature of these figures is the existence of a maximum of the liquid fraction in the centre of the tube, with a continuous shrinking and peaking of the zone of high liquid content and a progressive depletion of the region close to the wall from liquid. Meanwhile, the

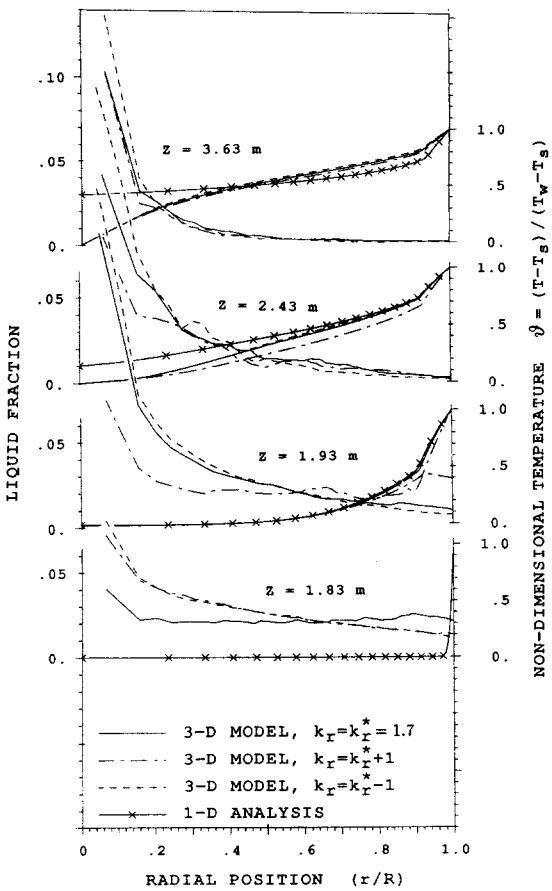

Fig. 6. Radial liquid fraction and vapour temperature distributions for test $U137_6$.

radial temperature profile shows a decrease of the gradient in the wall layer. This is due to the fact that, under the effect of the radial forces, the droplets tend to cluster around the centre of the tube: the interfacial heat transfer becomes more inefficient, as the droplets occupy regions where the vapour temperature is low.

The high liquid concentration in the centre of the tube causes the vapour to remain saturated there, and the concentration of heat sink in the central region results in large temperature gradients near the centre. The clustering of droplets in the centre is thus the phenomenon that causes low interfacial heat transfer in comparison to the case with droplets uniformly distributed across the channel.

The calculation also suggests that small droplets are more prone to drift towards the centre than larger ones. The projection of droplet trajectories on the cross section (Fig. 7) shows clearly the dependence of radial migration on droplet size. In Fig. 7 the calculated positions of the centres of droplets of different sizes are tracked in the r–ϕ plane. Figure 7(a) shows the case of a very small droplet (50 μm). The trajectory is heavily influenced by the turbulent eddies in the region immediately above the quench front.

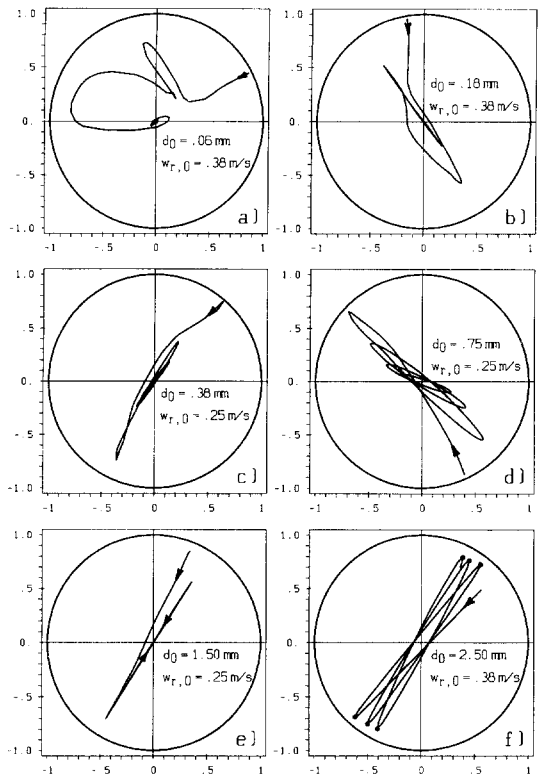

Fig. 7. Droplet trajectories in the cross-sectional (r–ϕ) plane of droplets of different sizes for test U137$_6$ (reference calculation).

The effect of turbulent fluctuations has become already quite small for a droplet of 170 μm, as can be recognized (Fig. 7(b)) from the relatively straight trajectory during the initial droplet motion. This droplet cannot reach the wall, as it is repelled by the thrust force, and is rapidly reaching the centre downstream from the entrance length.

The following droplet (Fig. 7(c)), 380 μm in diameter, has an initial positive radial velocity and collides with the wall very early. Its velocity is practically unchanged after the impact (the impact Weber number is very low, so that the restitution coefficient is one), but cannot impinge again on the wall, as its velocity is reduced by the drag force and inverted near the wall by the simultaneous effects of lift and thrust forces. The droplet moves again towards and oscillates around the centre; its radial velocity is not zero at the tube exit.

The 750 μm droplet (Fig. 7(d)) has a diameter close to the Sauter mean diameter of the droplet population at the tube exit. It is hardly affected by the turbulent eddies, and arrives nearly to touch the wall (only a few microns separate the droplet from the wall) at an elevation (z = 2.06 m) already above the entrance length. In this case, the initial radial momentum is almost sufficient for overcoming the forces pushing the droplet away from the wall. Further up, the droplet is decelerated by the drag force, moves on a elliptical orbit around the centre, and can no longer arrive so close to the wall. What is important to remark here, is the capability of this droplet to penetrate several times regions at high temperature, where its contribution to the cooling of the vapour can be significant.

The path of a droplet of 1.5 mm is shown in Fig. 7(e). The droplet is in contact with the wall already at birth, and is further decelerated by the drag force, so that it has no sufficient momentum for depositing again on the wall. It starts oscillating along a straight trajectory passing through the centre, in a radial region between one-half and two-thirds of the tube radius.

The last sample droplet shown (2.5 mm; Fig. 7(f)) is already a little larger than the largest droplet found in the experimental distribution. Droplets of such size, ejected with moderately high radial velocity ($\approx$ 1/10th of the axial velocity), have sufficient radial momentum, so that the radial forces cannot decelerate them much within an axial distance of about 2 m. Such droplets impinge on the wall several times, even with reduced velocity. This can be seen from the increase of the minimum centre-to-wall distance during the impact; in the first contact, the radial deformation is larger than in the following ones.

The fact that larger drops are less prone to radial drift towards the centre, where they are less effective in desuperheating the vapour, leads to an important consequence: the total interfacial heat flux does not depend only on the average diameter, but also on the radial distribution and history of the entire droplet population.

The considerations above explain the calculated wall temperature trends for test U126 (Fig. 8(a)), for the three different values of k_r. Fig. 8(b) shows that for k_r^*+1 (large radial velocities) the Sauter mean diameter (controlled by wall-impact break-up) decreases more than in the other cases. The lowest droplet size produces the lowest interfacial heat transfer and the highest exit vapour temperature. One-dimensional models would have predicted the opposite trend.

From the discussion above, it appears that the role played by the average droplet diameter is much more complex than that predicted by 1-D models, where the smaller the diameter, the larger the interfacial heat transfer and the desuperheating effectiveness of the droplets.

4.2. *Summary of the results and limitations of the model*

The results obtained by the model described in the companion paper [1] are generally in good agreement with the experimental wall and vapour temperatures for all the tests listed in Table 1, spanning over wide ranges of variables [3]. The agreement of the calculations with the data did not show any dependence on pressure. Generally, the model tends to overpredict the vapour temperature; the largest deviation was, however, less than 40 K. Large discrepancies in the

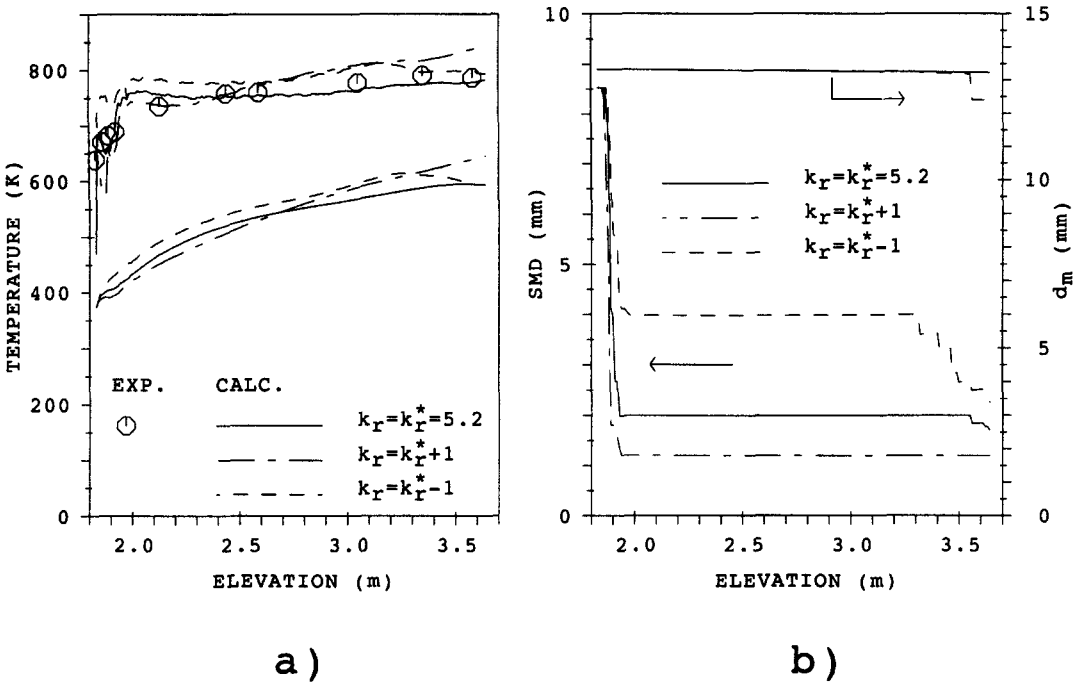

Fig. 8. (a) Effects of the droplet spectrum. Measured and calculated wall and vapour temperatures for test U126 ($p = 1$ bar; $G = 73$ kg m^{-2} s^{-1}, $x^+ = 0.04$), for three values of k_r; (b) axial evolution of the Sauter mean diameter SMD and maximum droplet diameter d_m.

calculated wall temperatures appear most of the time only in a 30–40 cm zone above the quench front, and agreement improves substantially at larger distances. The largest discrepancy far from the quench front was of about 70 K for the rather high mass flux test U136.

An appropriate estimation of the maximum initial radial velocity of the droplets is, however, essential for good predictions. The dependence of the results on the initial radial droplet velocity (unique adjustable parameter k_r) is the strongest at very low qualities (e.g. Fig. 9) and is practically negligible at high quality (e.g. Fig. 10). The influence of this parameter is due, to a large extent, to its capability to change the relative importance of the three break-up mechanisms considered. Large values of the initial radial momentum lead to an increased influence of wall-impact break-up (see above for test U137$_6$), which occurs within a short distance above the quench front, and to a reduced importance of the other two mechanisms (capillary and aerodynamic break-up), which modify the droplet spectrum in a much more gradual way. The importance of the initial radial droplet velocity is due to the assumed existence of large chunks of liquid above the quench front, as only large droplets can break up upon impact with the wall.

At low mass flux and low quality (e.g. test U351) capillary break-up has a predominant role (see Section 5) and reduces the average droplet diameter substantially within short distances, with important consequences on the heat transfer processes (controlled by the reduction in the interfacial heat transfer distance from the quench front). These effects appear

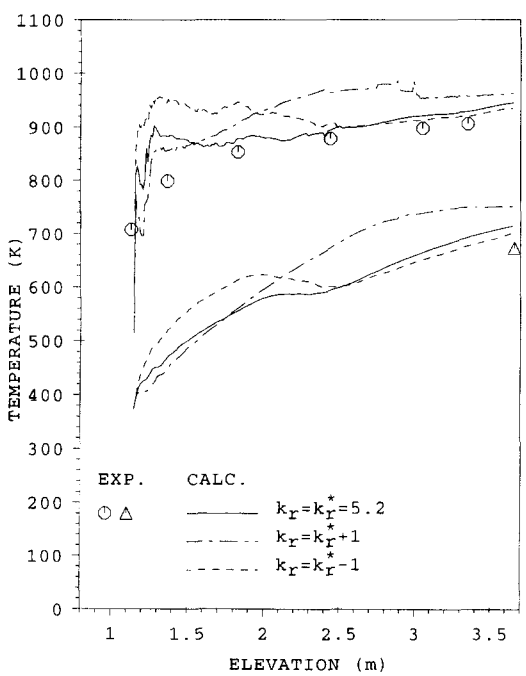

Fig. 9. Effect of the initial radial droplet velocity (value of k_r) for the *low quality* test U137$_3$, ($p = 1$ bar; $G = 75$ kg m^{-2} s^{-1}, $x^+ = 0.04$). Measured and calculated wall and vapour temperatures.

to be equally well predicted for the three values of k_r. The adequacy of the models for droplet break-up will be discussed in Section 5.1, where parametric studies concerning the break-up mechanisms are presented.

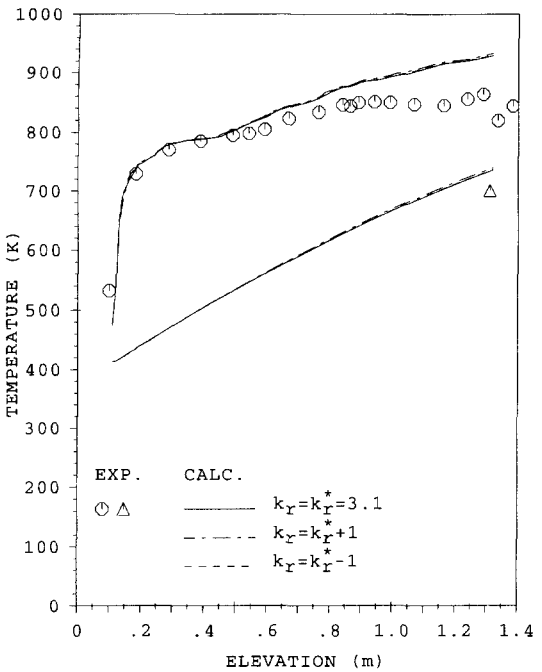

Fig. 10. Effect of the initial radial droplet velocity (value of k_r) for the *high quality* test L100 ($p = 3.8$ bar; $G = 14.8$ kg m^{-2} s^{-1}; $x^+ = 0.64$). Measured and calculated wall and vapour temperatures.

The initial Sauter mean diameter and velocities of the droplets are calculated using correlations developed for limited ranges of conditions. Thus, parametric studies are required to investigate the effect of these initial conditions on droplet hydrodynamics. Indeed, it has been found that, in spite of the use of the high drag coefficients typical of densely packed rigid spheres in granular flow or fluidized beds (Part I), the average void fraction above the quench front remains quite low over a long distance for many tests at low mass flux, as the droplets cannot be accelerated. This suggests that the Sauter mean diameter of the droplet population at the quench front may be overestimated, with important consequences on the fragmentation processes and the droplet histories further up. The effects of using correlations yielding smaller initial drop diameter is thus to be investigated.

So far, it has been shown that the good results obtained by the present model are due to its ability to predict much lower interfacial heat transfer rates than those obtained in a conventional 1-D calculation, as a result of the build-up of a highly non-uniform distribution of liquid over the cross section of the channel. The evolution of the droplet population size distribution seems also to play an important role, due to the different radial positions occupied preferentially by droplets of different diameters. These results somewhat depend on the assumptions used: some of them (such as the use of the same axial velocity for all the droplets) are supported by the experimental evidence, but some others need to be discussed.

When the packing limit is reached in the centre of the tube, the assumption of limited importance of the collision–coalescence phenomena used in this work does not hold any longer. Moreover, under high liquid loading conditions, the vapour velocity profile may be significantly altered, and even become concave; under these circumstances the lift force (which depends on the velocity gradient) would rather push the droplets away from the centre, and would cooperate with collision-induced diffusion to reduce droplet clustering. The classical single-phase two-layer undisturbed flow velocity profile used here is, on the contrary, convex and always produces a lift force which enhances the accumulation of droplets around the centre.

In summary, the present model predicts the *largest possible reduction of interfacial heat exchange due to the two-dimensional effects*. Therefore, if indeed the joint effects of the vapour velocity profile modification and collision-induced diffusion were limiting the liquid accumulation substantially, the calculated wall and vapour temperatures would have been overpredicted and should be regarded as conservative estimates. The assessment carried out shows, however, that the predicted values are near reality for most cases, even when such mitigating effects can be expected to be important.

On the other hand, the neglect of these liquid redistribution mechanisms might be the cause of the failure of the model in predicting the vapour and wall temperatures in two cases, namely at high mass flux (U136) and at very low quality ($U194_6$). The global success of the model for low mass flux and low-to-moderate quality conditions discouraged further efforts to consider these effects, as the knowledge of the collision–coalescence phenomena and of the flow structure under dispersed flow conditions is rather sketchy, and it can be implemented only at the cost of large coding complications.

The large contribution of radiative heat transfer to the total wall heat transfer rate (shown in Fig. 2), which was already recognized by Peake [8], poses additional problems in assessing the model. A substantial overprediction of the radiative heat transfer to the droplets could compensate for an irrealistically low interfacial heat transfer. The uncertainty stems from the observation that the radiation model used in the present study is based on assumptions that are not found to be true under most of the conditions investigated. The estimation of the error in the radiative heat fluxes is beyond the scope of the present work; more accurate results can be obtained only by using very sophisticated analytical techniques.

On the other hand, the model presented here needs a fitting parameter (k_r) to produce the good results shown above. Even for largely different radiative heat fluxes (as could have been predicted by a hypothetical better radiation model), alteration of the value of such a parameter would have still allowed (presumedly) to get the calculated results close to the experimental values under most conditions. Therefore, the conclusion that the 3-D model (allowing clustering of the

droplets in the central region of the channel) provides good predictions that are not possible with a 1-D model is not vitiated by the rough calculation of the radiative heat fluxes. Moreover the main conclusion of the study, that the 3-D approach is superior to any 1-D model *for low mass flux/low quality conditions*, will be shown not be influenced by the radiation model in Section 6.

5. PARAMETRIC STUDIES

The success of the model in predicting wall and vapour temperatures is largely dependent upon the appropriate choice of the unique free parameter, the initial radial droplet velocity, even though the results are not very sensitive to moderate variations ($k^* \pm 1$). Many empirical constants, however, had to be entered in the model. The study of their effect on the results is essential to the understanding of the level of detail required for a satisfactory simulation. Parametric studies concerning break-up processes and droplet size distribution are given first, and the influence of the controlling parameters is discussed. The parameters affecting other submodels are then briefly discussed.

Table 3. Effect of the values of the aerodynamic break-up parameters on the Sauter mean diameters d_{32} and maximum diameters d_m at the tube exit

Test no.	Break-up parameters We_{cr}	$e_{a,fr}$	k_r	Break-up mechanism	d_{32} (mm)	d_m (mm)
U126	12.0	0.2	5.2	wall	1.7	13.2
	5.5	0.2	2.0	aerodynamic	1.1	8.4
	5.5	0.5	2.0	aerodynamic	2.1	5.4
(exp.)					(1.9)	(3.7)
U137	12.0	0.2	2.0	aerodynamic	1.0	5.5
	5.5	0.2	2.0	aerodynamic	0.6	4.4
	5.5	0.5	2.0	aerodynamic	0.8	2.8
(exp.)					(0.9)	(2.3)
U194	12.0	0.2	5.2	capillary	0.6	4.4
	5.5	0.2	2.0	aerodynamic	1.0	6.4
	5.5	0.5	2.0	aerodynamic	1.7	4.1
(exp.)					(1.8)	(4.6)

For each test, the first line gives the results of the basic model, the second and third the results obtained by forbidding capillary break-up and imposing $k_r = 2$, which reduces, wall-impact break-up near the quench front. In parentheses the experimental values of Peak [8].

5.1. *Influence on the break-up parameters*

Only the main results of this parametric analysis are summarized here, as a large part of the complete study [3] has already been presented and discussed elsewhere [10].

5.1.1. *Tests at moderate mass flux.* For the three experiments at moderate flooding rate (7.5 cm s^{-1}), for which the droplet size distributions at the tube exit were observed when the quench front was at about half height in the tube, quite irregular spectra were found. Indeed, distributions with several maxima were observed, which cannot be described by any of the usual equations for sprays. Although many mechanisms can be responsible for the observed 'irregular' droplet size distribution at the tube exit,† a certain credit can be given to the hypothesis that bag-type aerodynamic break-up caused the gap between the large fragments generated by the splitting of the liquid rim, and small droplets created by disintegration of the liquid sheet.

The *basic model* or *reference calculations* (with the aerodynamic break-up parameters calculated according to the criteria already discussed, and including the other two break-up mechanisms) predicted well the Sauter mean diameter, d_{32}, of these distributions in the first two of the three cases, but overpredicted the largest droplet size (d_m) in all cases (Table 3). For the three tests U126, $U137_6$ and $U194_6$, the droplet size evolution was controlled by wall-impact break-up, aerodynamic break-up and capillary break-up, respectively.

To find out whether aerodynamic break-up *alone*, possibly with adjusted parameters, can produce an adequate droplet population evolution in all cases, sensitivity studies were carried-out by altering the parameters which control aerodynamic break-up, namely the critical Weber number We_{cr} and the ratio between the diameters of the daughter and parent droplets, $e_{a,fr}$. For these parametric studies, capillary break-up was prohibited and wall-impact break-up was reduced to the minimum expected, corresponding to the value of the radial velocity multiplier $k_r = 2$. After a few trials, it was found that excellent agreement for *both* Sauter mean diameter and d_m *could* be obtained (Table 3) by reducing We_{cr} to 5.5 (the lowest value reported by Sarjeant [11]) and increasing the size of the largest fragment to half the diameter of the parent drop (value reported by Pilch and Erdman [12]). The destabilising effect of the presence of adjacent droplets in a cluster could be the physical reason for the lower values of We_{cr} suggested by these studies.

Surprisingly enough, wall and vapour temperatures were, on the other hand, hardly affected. Similar results have been obtained for several other cases at *moderate mass flux*: the altered values of We_{cr} and $e_{a,fr}$ produced only slight differences in the temperatures, in some cases improving a little the predictions. Several compensating mechanisms in the calculation of the interfacial heat flux q_i'' are at the origin of this finding [10].

5.1.2. *Tests at low reflooding rate.* Tests at *low mass flux* and low (and also moderate) quality show quite a different trend. In the reference calculations, which gave good results for wall and vapour temperatures, the droplet size evolution was controlled by the capillary break-up mechanism. Dramatic underprediction of the temperatures is observed for tests U122 and

† Imperfect statistical sampling of the flow could also have played a role, of course.

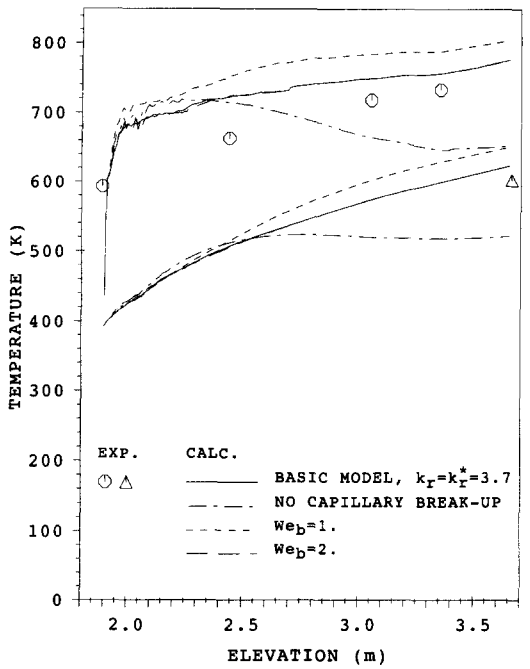

Fig. 11. Effect of using different options for capillary break-up on the wall and vapour temperatures for the low mass flux U351 ($p = 2$ bar; $G = 25.1$ kg m^{-2} s^{-1}, $x^+ = 0.12$).

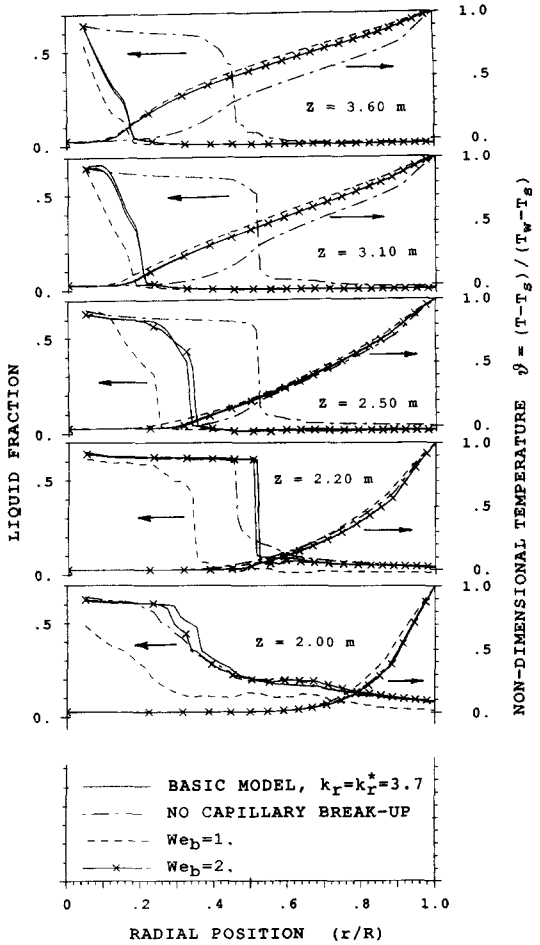

Fig. 12. Effect of different options for capillary break-up on the radial liquid fraction and vapour temperature profiles for test U351.

U351 (Fig. 11 refers to Test U351), when capillary break-up was prohibited, as the size of the droplets, in the absence of capillary break-up, is much larger now than in the reference calculations. This result was independent of the choice of the parameters for aerodynamic break-up.

For these tests, the lack of a mechanism that reduces quickly the drop size above the quench front (and results in accumulation of the droplets in the centre of the channel where interfacial heat transfer is low, as shown in Fig. 12) produces totally wrong predictions, due to the overestimation of the interfacial heat transfer. This parametric study shows that a break-up mechanism *different* from aerodynamic break-up *must* take place under low mass flux conditions, while the *We* is still low.

Summary. The use of a lower value for the critical Weber number ($We_{cr} = 5.5$) and of a larger value for the diameter of the largest fragment ($e_{a,fr} = 0.5$) allows a more realistic prediction of some tests at moderate mass flux and of some at moderate quality, but for most tests no substantial difference is observed. For *low mass flux/low quality* conditions, aerodynamic break-up alone does *not* yield good predictions, irrespective of the choice of the break-up parameters.

5.2. *Droplet volume distribution*

The negligible effect of the aerodynamic break-up parameters on the temperatures, obtained in spite of their large impact on the droplet size distribution, suggested a more general investigation of the effects of the droplet spectrum.

Several tests have been analysed by *prohibiting break-up*, but using for the initial Sauter mean diameter and d_m the values obtained in the reference calculations (*with* break-up) *at the exit* of the tube (superscript $^{T^*}$ in the figures below). These runs have been carried out with both an upper-limit-log-normal distribution (ULLND in the figures below), as well as a Nukiyama–Tanasawa [13] distribution (NTD in the figures below).

The same tests have also been analysed using a unique *initial* droplet diameter, imposed as the Sauter mean diameter at the tube exit obtained in the reference cases (calculations identified by label $d_k = \mathrm{SMD}^{T^*}$). These calculations were repeated with a modified value of the initial radial droplet velocity $w_{r,0}$ (label $k_r = 2$).

For all tests, the calculations performed with a spectrum of sizes (upper-limit-log-normal and Nukiyama–Tanasawa distributions) do not show any substantial difference. The only appreciable changes in the wall and vapour temperature trends occur in vicinity of the quench front: at some distance from the quench front, the effect of the particular distribution practically vanishes.

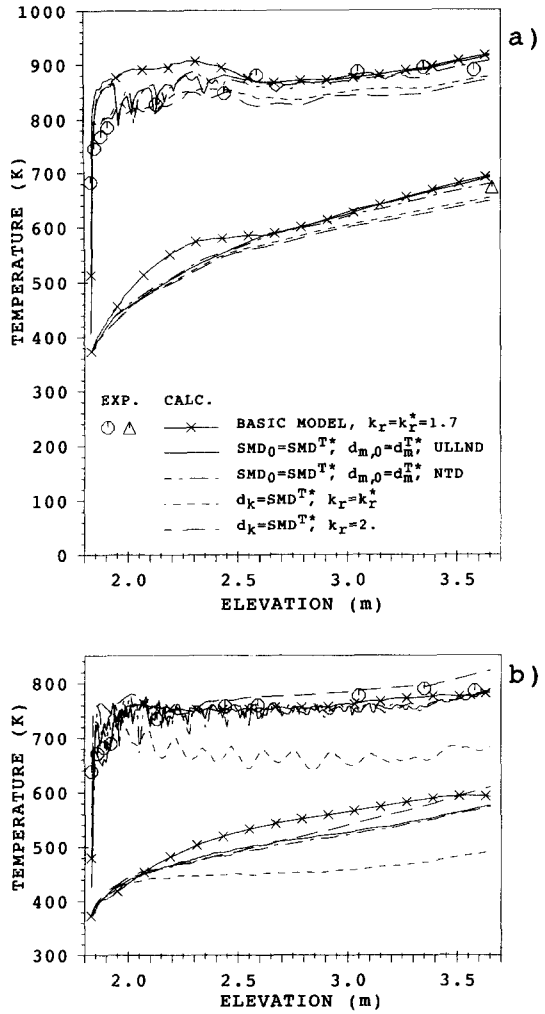

Fig. 13. Effect of different droplet size distributions with $SMD_0 = SMD^{T*}$ and $d_{m,0} = d_m^{T*}$ for : (a) test U137 ($p = 1$ bar; $G = 75$ kg m^{-2} s^{-1}; $x^+ = 0.09$) and (b) test U126 ($p = 1$ bar; $G = 75$ kg m^{-2} s^{-1}; $x^+ = 0.04$).

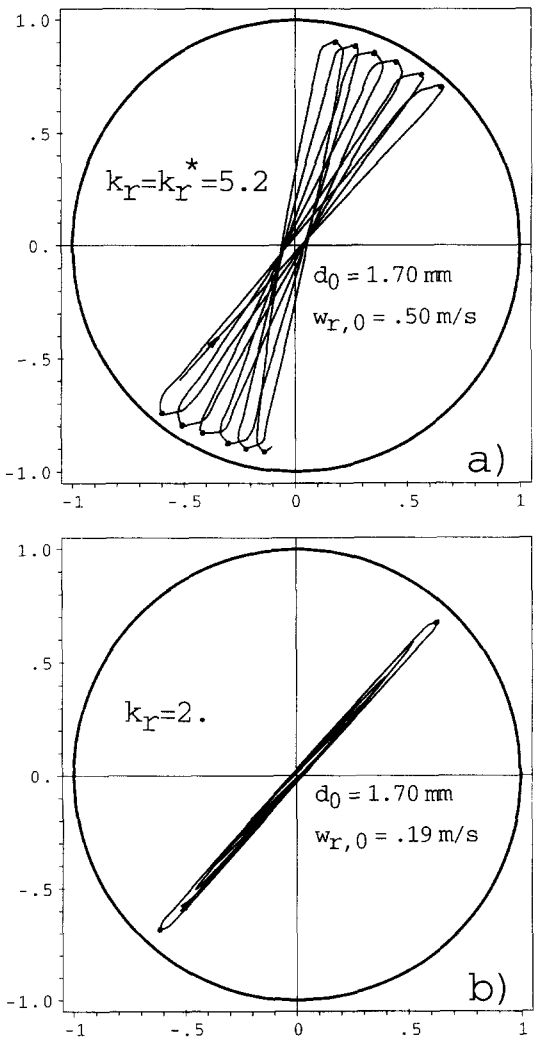

Fig. 14. Trajectory of a droplet for test U126, when all the droplets have the same diameter SMD^{T*}, for two values of k_r.

Two different trends are recognized, however, when the unique initial value SMD^{T*} is imposed to *all* droplets. For test U137, the wall and vapour temperature profiles are practically the same as those calculated with a spectrum of droplet sizes, while large differences exist for test U126 (Fig. 13). In this second case, large deviations from the reference results (and from the experimental ones) have been obtained, and the predictions are largely dependent on the initial radial droplet velocity.

The different trends for the two tests can be explained by considering the calculated average droplet size (imposed to all the droplets) which was much larger for test U126 than for test U137. In this second case, the small droplets are easily rejected from the wall under the combined effects of drag, lift and wall reaction forces, and migrate towards the centre where the vapour temperature and, consequently, interfacial heat transfer are low. Under these circumstances, even a very large difference in droplet size distribution and initial radial momentum produces only a small effect.

On the other hand, the large droplets for test U126 have an inertia large enough for touching the wall several times, as the projection of the droplet trajectory on the cross-sectional plane in Fig. 14(a) shows. The drops stay longer in the high vapour temperature, near-wall region of the channel, causing high interfacial heat transfer and thus reducing wall and vapour superheats. The radial momentum and, consequently, the capability to touch the wall are, obviously, also dependent on the radial velocity, so that the sensitivity of the results to the initial radial droplet velocity can also be explained. Figure 14(b), showing the trajectory of the droplet for a reduced value of the initial radial velocity $w_{r,0}$, illustrates this finding.

5.3. *Initial void fraction*

With the present model, as mentioned in Section 4.2, at low mass flux the droplets cannot be accelerated immediately above the quench front, but instead are slowing down, up to the elevation where the strong

void fraction effect on the drag coefficient for fluidized beds balances the drag and gravity forces. The lowest value of the void fraction can be 20% less than the initially imposed void fraction just below the quench front, $\langle\alpha_g\rangle^-$, calculated by Ishii's correlation (Part I—reference calculations). For these conditions, one is led to conclude that, in reality,† either the initial void fraction is lower, or the initial value of the Sauter mean diameter is much smaller than that predicted assuming entrainment from roll-waves.

Parametric studies have been performed for several runs, using either the Lellouche–Zolotar correlation [14] which yields larger $\langle\alpha_g\rangle^-$, or the EPRI drift-flux model [15], which yields lower values than the Ishii correlation used in our basic model. The results show that for a low velocity ratio (high void fraction) at the quench front, the 3-D model overpredicts the tests at low mass flux, while slight improvements with respect to the reference calculations can be obtained for larger values. The sensitivity of the model to the initial velocity ratio is thus quite high: only large values (which are expected to be more realistic) allow good predictions, whereas low values yield too high temperatures.

5.4. *Initial Sauter mean diameter for low mass flux tests*

So far, the Sauter mean diameter at the quench front has been calculated according to the empirical formula of Ardron and Hall, even for conditions (mass flux, quality and pressure) outside their database. It has been observed that, while the presence of large droplets in tests at moderate mass flux (>40 kg m^{-2} s^{-1}) is consistent with a model that considers aerodynamic break-up,‡ several difficulties are encountered in justifying large droplets at low mass fluxes, especially at pressures higher than atmospheric. For the latter condition, if no other mechanism provokes break-up, large droplets can travel along distances without becoming unstable, and produce a fairly uniform distribution of the liquid fraction over the cross sectional area and underprediction of the temperatures. To avoid this effect, a capillary break-up process was introduced. The assumption of an increased importance of capillary break-up (seldom observed at higher mass fluxes), serves only as a rationale for the rapid droplet size reduction that is required to get good agreement between calculated and experimental wall and vapour temperatures.

However, it is also possible that much smaller droplets than those predicted by the Ardron and Hall correlation could be generated at the quench front at low mass fluxes. Since the same difficulties are encountered at very low quality, i.e. low vapour flux (test U194$_6$), one could assume that a *different generation mechanism is present at low vapour mass fluxes.*

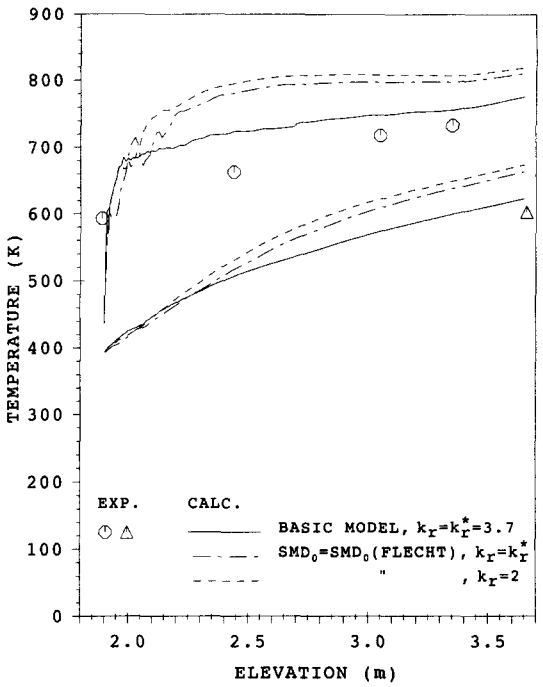

Fig. 15. Effect of a reduced value of SMD_0 (calculated from the FLECHT correlation) for the low mass flux test U351 (p = 2 bar; G = 25.1 kg m^{-2} s^{-1}; x^+ = 0.12).

To test the effect of a smaller initial Sauter mean diameter, the FLECHT correlation [16], derived from rod bundle experiments *under low mass flux conditions*, was used in the calculation of the low mass flux runs.§ According to this correlation, the largest droplet size at low gas flux depends only on the pressure, and is smaller than 2 mm at atmospheric pressure and even smaller at higher pressure.

Thus, six tests at low mass flux (U122, U351, U353, L114, L115 and L129) have been analyzed using the FLECHT correlation for the Sauter mean diameter, for two different values of k_r. No break-up was allowed in these calculations. Results were quite contradictory: while for tests U122 and L115 the calculations give results very close to the reference ones, large overpredictions of wall and vapour temperatures are calculated for the other tests at low mass flux (e.g. Fig. 15 for test U351). These results, due to a reduction in the Sauter mean diameter with respect to the reference calculation, can only be interpreted in light of the complex dependence of the liquid mass distribution, interfacial heat transfer, and wall-to-droplet radiative heat flux on droplet size. Thus, the results are consistent with the basic feature of the 3-D model: smaller droplet sizes can result in higher temperatures.

It is evident that for each low mass flux test, a best-

† According to the usual assumption that the largest droplet existing in the initial distribution should be sufficiently small for being lifted by the drag force [9].

‡ Wall-impact break-up becomes also important, if the conventional limit, We_{cr} = 12, for single droplets is used to define the criterion for aerodynamic break-up.

§ Many other correlations have been considered [3], but all of them yield droplet diameters which depend on the main parameters in a way similar to that of either the FLECHT correlation or the correlation of Ardron and Hall [17] used as the reference, or produce unrealistically large droplets.

fit Sauter mean diameter value can be found: a low value for the initial droplet diameter is, however, not a solution for all cases. On the other hand, an equation for the initial Sauter mean diameter adequately covering all conditions, i.e. correlating the Sauter mean diameter with pressure, mass flux and quality has not been developed yet.

Therefore, it is not clear whether, under low gas flux conditions, large droplets can exist above the quench front and then break further up, or whether only small droplets are generated at the quench front, their Sauter mean diameter being dependent on several parameters. More experimental work is needed to provide the basic understanding for the droplet generation mechanism at low gas flux conditions.

Summary. In the absence of an appropriate correlation yielding small values for the initial Sauter mean diameter under low vapour flux conditions, the presence of capillary break-up is necessary for reducing the initially large size of the droplets and producing good predictions.

5.5. *Interfacial heat transfer coefficient*

The choice of the modified Beard–Pruppacher correlation for the interfacial heat transfer coefficient $h_{0,k}$ (Part I) has been somewhat arbitrary, and motivated by the opportunity to compare the 3-D calculations with 1-D calculations. (Section 6) *while minimizing* interfacial heat transfer. In the previous sections, it has been shown that the small droplets (which have a large $h_{0,k}$) are carried towards zones of low temperature, where (whatever the correlation used) they do not contribute substantially to the heat sink. Vice versa, large droplets, which can move undisturbed across the tube contribute heavily to interfacial heat transfer. However, the $h_{0,k}$ for large drops does not depend much on the correlation used, at least at terminal speeds [3]. Therefore only a small sensitivity of the calculations to the correlation for $h_{0,k}$ can be expected. Sensitivity analyses are interesting anyway, as the impact of the choice of the correlation can be compared with its impact on the 1-D models, which was found to be rather high, even for the high void fraction conditions characterizing test U137 [3].

Ten tests have been analyzed with different combinations of choices for the interfacial heat transfer coefficient $h_{0,k}$ and the correction factors (Part I).† In all cases (but for test L129, where the average void fraction stayed at a low value up to the tube exit) wall and vapour temperatures were in a band of 40 K.

In general, it can be concluded that within the reasonable limits investigated, the role of the interfacial heat transfer coefficient in the 3-D model is much less important than that of other closure laws, like the ones yielding the Sauter mean diameter and the initial void fraction.

† In the authors' opinion the correlation by Renksizbulut and Yuen [8] is the most appropriate one.

‡ The standard choice of the present model.

5.6. *Radial forces*

A discussion of the forces that act radially on the droplets has been presented in Part I. It has been remarked that no general agreement exists for both the form and the strength of the lift and thrust forces, and that the application of theoretical and experimental results obtained for rigid spheres to deforming large droplets is somewhat arbitrary. To understand to what extent the radial forces affect droplet hydrodynamics and *the relative importance of lift and thrust forces* in flows with large radial velocity or temperature gradients, two tests which exhibit these two features, $U137_6$ and I222 respectively, are investigated. For test $U137_6$ the Reynolds number (≈ 5700 at the tube exit) is low producing a high velocity gradient and the heat flux is moderate (low temperature gradient). Test I222 was characterized by high heat flux (high temperature gradient) and fully turbulent flow (low velocity gradient).

Parametric calculations have been carried out as follows: the lift force has been assumed to be zero, and the thrust force has either been neglected, or calculated according to the two different expressions of Ganic and Rohsenow [19] or of Lee and Almenas [20]. It is observed that, if both radial forces are neglected, large underpredictions of both wall and vapour temperatures are obtained, so that the consideration of radial forces that push away the droplets from the wall must be an important feature of the present model. The thrust force alone, as expressed by the equation of Lee and Almenas, can produce most of the heat sink degradation that causes the higher temperatures observed in the experiment. However, if the thrust force acts only in the viscous layer, as implied by the expression of Ganic and Rohsenow, such a heat sink reduction effect vanishes, and the calculated temperatures overlap the results obtained when only drag is considered. Then, *in order to get the correct reduction of interfacial heat transfer, radial forces must act over a large part of the cross section, and not only close to the wall*, so that the droplets remain within a central area smaller than the turbulent core of the flow.

Additional parametric studies have been focussed on the influence of the lift force alone: the two expressions of Rubinow and Keller [21] and Saffman‡ [22] were tested in the absence of a thrust force. It was observed that, independently of the expression chosen, the lift force alone can produce the correct radial distribution of liquid, and thus the right wall and vapour superheating.

This holds also for higher Reynolds numbers (smaller velocity gradients), as it could be verified for test I222. In this case, overlooking the presence of *either* thrust or lift force, results in practically the same predictions of both vapour and wall temperatures. Vice versa, if *both* are eliminated, the vapour temperature is underpredicted by more than 100 K.

It follows that *independently of the origin of the force* (lift or reaction force), *good results can be achieved*

only if a centripetal force of the order of magnitude of those considered in the present model constraints the droplets near the centre of the channel.

5.7. *Initial tangential velocity*

The droplets have been viewed as being ejected from the liquid film practically normal to the wall, as their tangential velocity $w_{k,t}$ has been at most 1/10th of their initial radial velocity. It is of some interest to appraise the effect of an increased tangential velocity.

Two calculations have been carried out for test $U137_6$, with the tangential velocity allowed to be at most equal to the radial velocity: one with the full model, another neglecting lift and thrust forces (drag only). It was observed [3] that, when the radial forces were considered, practically no difference existed in comparison to the case with small tangential velocities; the effect of the radial forces overcomes the effect of the initial conditions. On the other hand, if drag is the only active force, a certain influence of the initial tangential velocity is found, even though of much smaller magnitude, compared to the effect of the radial forces. The differences in the temperature profiles can be explained by considering the effect of the forces on the radial liquid distribution: when the radial forces are present, the profile has the same peak in the centre and it is practically unaffected by the initial direction of flight of the droplets.

Without radial forces, and for low initial $w_{k,r}$ the liquid fraction profile is not sufficiently peaked in the centre. A nearly uniform void fraction distribution is calculated if the initial tangential velocity is large.

Tangential velocities, then, play a minor role when strong centripetal forces act on the droplets.

5.8. *Influence of the packing limit*

All the calculations have been carried out assuming that the clustering of the droplets around the centre is limited by the maximum admissible packing for solid spheres, which is about 0.6. However, already at much lower liquid fractions, collisions occur between the droplets, so that a collisional diffusion mechanism prevents a very tight packing. Collisions are not accounted for in the present model and diffusional spreading of the liquid mass is artificially obtained by the procedure described in Part I, which substantially consists of a redistribution of the droplets among the radial nodes, until the liquid fraction in each node is larger than the packing limit $\alpha_{f,m}$. Since $\alpha_{f,m}$ was arbitrarily selected, a sensitivity study is in order.

Figure 16 presents wall and vapour temperatures for test U351, with values of 0.4 and 0.6 imposed to $\alpha_{f,m}$. No large differences exist with respect to the reference calculation ($\alpha_{f,m} = 0.6$), even though a certain decrease of the temperatures is found, as expected. Of interest is the comparison of the void fraction profiles at different elevations for the two values of $\alpha_{f,m}$ (Fig. 17). The radial distribution of liquid is affected quite heavily by the change of the packing limit, without a correspondingly marked

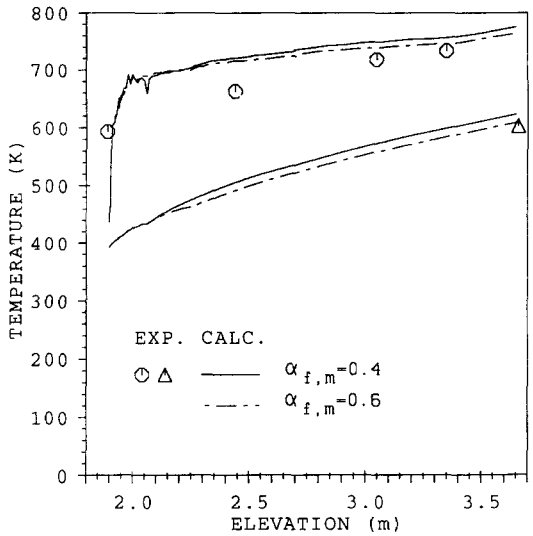

Fig. 16. Effect of the largest admissible liquid fraction $\alpha_{f,m}$ on vapour and wall temperatures for test U351.

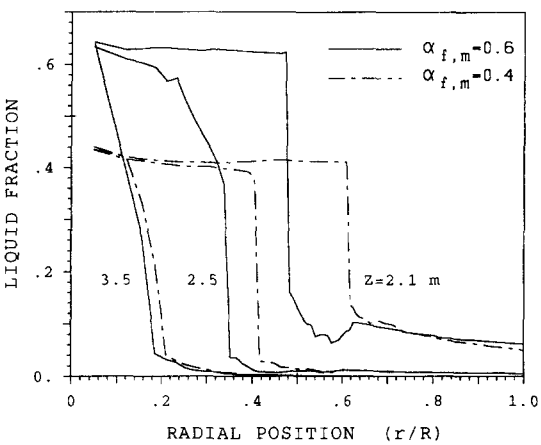

Fig. 17. Effect of $\alpha_{f,m}$ on the liquid fraction profiles for test U351.

change of the global cooling capability of the liquid. In both cases, a large zone close to the wall, larger than the viscous layer, is completely depleted of droplets.

This result leads to the conclusion that *the redistribution of liquid among the central zones has a minor influence on the total interfacial heat transfer, which, on the contrary, is affected only by the presence of the droplets in the near-wall high temperature regions.*

6. COMPARISON TO ONE-DIMENSIONAL ANALYSES

The model developed here is quite detailed, and the need for such a level of complexity must be justified. In order to show that good results can be obtained only if the multi-dimensional effects are properly taken into account, the results of the new model were compared with those obtained by a 1-D model.

A one-dimensional model can readily be obtained from the vapour mass and energy conservation equa-

tions (equations (1)–(3) in the companion paper), by imposing cross-sectionally constant vapour generation rate Γ, interfacial heat transfer per unit volume q'''_{gi} and local void fraction α_g. It can be shown [3] that the modified conservation equations yield the same bulk vapour temperature T_b and wall temperature T_w as those obtained by a standard 1-D model employing, however, the wall-to-vapour heat transfer coefficient calculated from the actual radial vapour temperature profile accounting for the presence of droplets. This temperature profile can be obtained from separate 2-D calculations [3]. The cross-sectionally constant values of Γ, q'''_{gi} and α_g must be taken as:

$$\Gamma = \frac{1}{H_{fg}}\left[- \langle Q_{ig} \rangle + \frac{4}{D}(q''_{wf} + q''_{gf}) \right] \tag{3}$$

$$q'''_{gi} = \langle q'''_{gi} \rangle = - \langle Q_{ig} \rangle \tag{4}$$

$$\alpha_g = \langle \alpha_g \rangle = \frac{\langle x \rangle}{\langle x \rangle + \dfrac{U_z}{W_z}\dfrac{\langle \rho_g \rangle}{\rho_f}(1 - \langle x \rangle)} \tag{5}$$

where $\langle x \rangle$ is calculated from:

$$\langle x \rangle = \frac{\dot{M}_g}{\dot{M}} \tag{6}$$

$\dot{M}_g \equiv A \langle \rho_g \rangle \langle \alpha_g \rangle U_z$ being the vapour mass flow calculated from equation (3) and $\dot{M}$ the total mass flow rate. The cross-sectional-average interfacial heat transfer per unit volume $\langle Q_{ig} \rangle$ is calculated from:

$$\langle Q_{ig} \rangle = \pi d^2 n h_i (T_b - T_s) = \frac{6(1 - \langle \alpha_g \rangle)}{d} h_i (T_b - T_s) \tag{7}$$

where d is the average droplet diameter and n is the droplet number concentration (droplets m^{-3}).

Under such conditions, equations (3)–(5) and (7) produce 'equivalent' 1-D calculations. The most important closure relation for a 1-D model is that for the droplet diameter, as the results are heavily influenced by its choice. Therefore, in order to compare the capabilities of the usual 1-D approach with those of the new model in a general sense, it is necessary to perform 1-D calculations using droplet diameters in a wide, though realistic range. The average droplet diameter was calculated according to the following four different sets of rules:

(a) The average diameter *at any elevation* is calculated from the aerodynamic stability criterion $d = We_{cr}\sigma/\rho_g U_{fg}^2$, where We_{cr} is set to 7.5. The initial value of U_{fg} is calculated using the same correlation (Ishii's) for the void fraction at the quench front, as that used for the basic 3-D model (see companion paper). The droplet diameter is allowed to be at most equal to one third of the tube diameter.

(b) The same rules are used, but with $We_{cr} = 22$, which is the largest observed critical Weber number for stable droplets.

(c) The *initial* droplet diameter d_0 is obtained from a balance between gravity and drag forces. Further up, the diameter is the lowest between the initial one and that dictated by the aerodynamic stability requirement (criterion under (a)).

(d) The same procedure is followed as in (c), apart from the choice of the correlation for the void fraction at the quench front. The drift flux model of Chexal and Lellouche [15] is used instead of the Ishii correlation; this yields a lower void fraction and a large initial droplet diameter than in analysis (c).

In general, analyses (c) and (d) should include an equation for the droplet diameter reduction along the channel due to evaporation (e.g. ref. [8]). However, for the range of conditions investigated in the present work, such a reduction can be neglected. When the number of droplets remains constant along the channel (no break-up), the droplet diameter is given by:

$$\frac{d}{d_0} = \left[\frac{1 - x}{1 - x_0}\right]^{1/3} \tag{8}$$

so that, up to high qualities, a moderate increase in x causes a small reduction of d. For the conditions investigated, the droplet diameter reduction along the tube would amount to no more than 14%, and can thus be neglected.

The four types of analyses (a)–(d) described above have been carried out for each of the 32 tests. The evaluation of the results permitted to identify quite large differences in the success of the predictions of the 1-D model. The void fraction just above the quench front $\alpha_g^+ \equiv \langle \alpha \rangle^+$, and the mass flux G seem to be the parameters that affect most the adequacy of the predictions. In the $G - \alpha_g^+$ map of Fig. 18 (where use of the void fraction immediately above the quench front α_g^+ allows to include the effect of pressure), three different groups of results and corresponding regions can be identified; these are distinguished by different symbols in Fig. 18:

(1) Empty symbols: the results of the 1-D analysis (a), i.e. for average droplet diameters between 1 and 2 mm, and to a lesser extent of analyses (c) and (d) agree reasonably well with the data. Large discrepancies are observed only for the largest droplet diameters (analysis (b)).

(2) Half-full symbols: the experimental results are in the range between predictions (b) and (d). For many of these tests, however, the calculated temperatures are lower than the experimental ones except for analyses (b), where the value of the droplet diameter at the exit is about one third of the tube diameter. A very large diameter is needed to obtain good results for high wall and vapour superheating; this generates some doubt about the validity of the 1-D approach.

(3) Full symbols: wall and vapour temperatures are underpredicted (in some cases by more than 100 K)

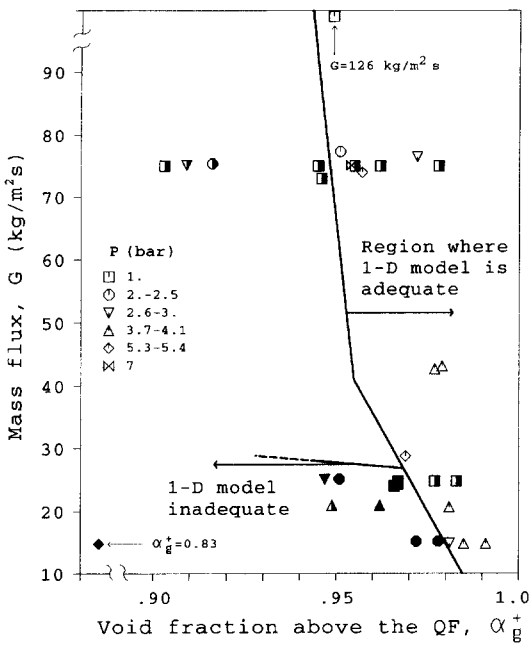

Fig. 18. Adequacy of the results obtained by the 1-D analyses (empty symbols—good results; half-full symbols—good results obtained for large droplet diameters; full symbols—bad results).

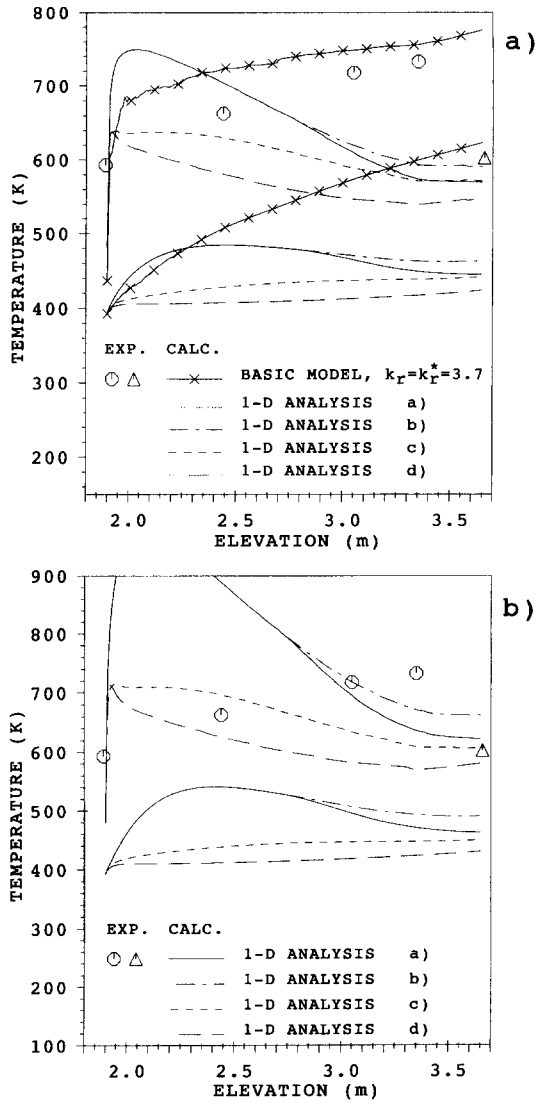

Fig. 19. (a) Comparison of wall and vapour temperatures calculated by the 3-D model with results obtained by 1-D analyses, and with experimental data, for the low mass flux test U351; (b) 1-D results when radiative heat flux is neglected.

in all the analyses, i.e. for any droplet diameter in the range between a few hundred microns and one third of the tube diameter. All the tests in this group are at low mass flux and low quality: for these tests the 1-D approach seems to be completely inadequate.

The existence of this last set of conditions for which the 1-D approach always underpredicts the temperatures, and the superiority of the new model under such conditions is the main result presented here. This finding is illustrated below, using as an example the 1-D results presented in Fig. 19(a) for the 2-bar reflooding test U351. For any (reasonable) choice of the droplet diameter, which is as large as 4.8 mm at the tube exit in analysis (b), the vapour superheat is underpredicted by at least 140 K or a factor of 2. This result is confirmed even when the effects of experimental and other uncertainties are considered. The results do not improve even when the radiation heat transfer is neglected, as shown in Fig. 19(b).

The strong underprediction of the vapour temperature is likely to be related to excessive interfacial heat transfer. Since already a quite low value of h_i was used, and even the use of large droplet diameters did not help, it can be concluded that, unless there is a gross error in the calculation of the drag force (and thus of the velocity difference between the phases from which h_i depends), it is the 1-D approach itself that overpredicts interfacial heat transfer.

The extensive parametric investigations carried out [3] clearly revealed that the predictions by the 1-D models become quite unreliable at low qualities and mass fluxes. On the contrary, for low mass flux tests, the results obtained by the present 3-D model are quite satisfactory, as shown in Fig. 19(a). The good prediction of the exit vapour temperature is due to a strongly reduced interfacial heat transfer (Fig. 20). The interfacial heat flux q_i'' for the 3-D calculation is lower than that obtained in analysis (b), in spite of the fact that the average vapour temperature is larger, and the Sauter mean diameter of the droplet population at the tube exit is much smaller than in the most favourable (case (b)) 1-D analysis (in that case the Sauter mean diameter at the exit was equal to 1/3 the tube diameter).

The reason for such a reduction in q_i'' can be found again in the clustering of the droplets around the centre (Fig. 12). The non-uniform distribution of the liquid over the cross section seems to be the only

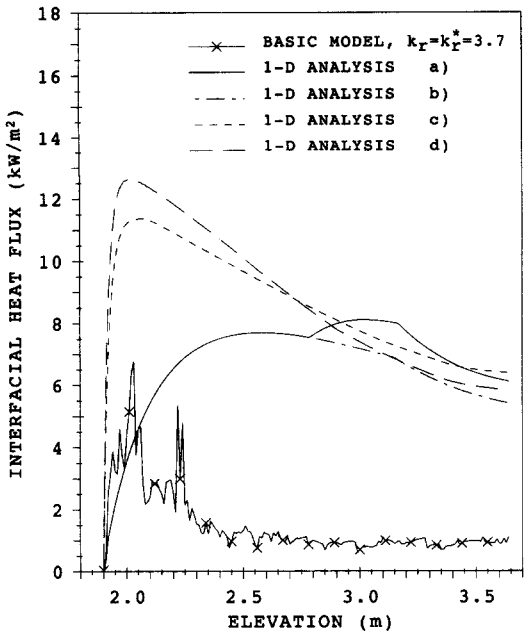

Fig. 20. Comparison of the interfacial heat transfer rate (per unit wall area) calculated by the 3-D model with that obtained by the 1-D analyses for test U351.

mechanism that can explain the high temperatures observed in the experiment.

7. PERFORMANCE OF THE 1-D MODELS IMPLEMENTED IN THE NUCLEAR SAFETY CODES FOR LOW MASS FLUX CONDITIONS

The main result of the present investigation is that the interfacial heat transfer is underpredicted by any 1-D model using reasonable values for the quench front conditions, interfacial drag, interfacial heat transfer coefficient heat transfer coefficient and droplet diameter. This has consequences for the computer codes used in the nuclear industry.

In fact, practically all codes use 1-D models for subchannel analysis (the 3-D representation refers to the core as a whole). Based on the results shown in the present paper, these codes are expected to largely underpredict the vapour temperatures above a slowly advancing quench front.

A first confirmation (or, at least, no counter evidence) of this expectation can be found in the recent results obtained with a modified version of TRAC (TRAC-PF1/MOD1) by Nelson and coworkers [23–25]. The vapour temperatures at the exit of a (1.156 m long) vertical tube under steady state conditions, was systematically underpredicted (standard deviation of the vapour temperature equal to 39%) for pressures between 2 and 10 bar and moderate mass fluxes (50–200 kg m^{-2} s^{-1}). The experimental value of the void fraction (>80%) suggests dispersed flow. The calculated flow pattern in the largest part of the post-critical-heat-flux zone was a so-called 'post agitated inverted annular flow regime', for which interfacial heat transfer and drag are calculated by weighting correlations for pure dispersed flow and complex regimes originating from the break-up of the liquid column. Therefore, the model for dispersed flow film boiling is not uniquely involved, and the low vapour temperatures calculated may be due to several reasons.

Unal *et al.* [25], report that also the calculations of some moderate mass flow transient reflooding tests performed in the UC-B test section (belonging to the same series of tests used for the assessment here) show a systematic underprediction of the vapour temperature.

A more direct confirmation of the fact that the 1-D models in the large computer codes have difficulties in predicting the vapour temperature for low mass flux tests has been obtained by calculations of tests U351 and U353 using RELAP5/MOD2.5 and RELAP-5/MOD3 [26]. Transient analyses, which produced a fast desuperheating of the vapour and a too large quench front velocity, were not very helpful in judging limitations of individual submodels, as many deficiencies in other models could be responsible for making the cooling rates of vapour and wall much faster than in the experiments. Therefore, calculations (quasi-steady state) with imposed time-independent axial wall temperature profiles and with the test section 'cut' immediately below the half length position, in order to impose the quality at the quench front, were performed. In spite of the oscillations present in all the variables, it could be recognized that the average values of the hydrodynamic boundary conditions (quality at the quench front, mass flow rate at the quench front and at the outlet) were close to the experimental values. Under these conditions, and for total heat inputs to the fluid above the quench front larger than in the experiment (Fig. 21), the calculated vapour temperature at the end of a short initial transient was underpredicted by at least 70 K (Fig. 22). For Test U353, the underprediction was as high as 110 K [26]. These results confirm that, unless the interfacial drag laws for dispersed flow have severe deficiencies, the interfacial heat transfer rate must have been overestimated.

The overprediction of the interfacial heat flux can thus be considered a common feature of all the 1-D models, and there is good evidence that this is an intrinsic inadequacy.

8. CONCLUSIONS

The main finding of this work is that, for low mass flux conditions, the conventional 1-D approach based on the assumption of uniform droplet distribution over the cross section and on the calculation of interfacial heat transfer using only cross-sectionally averaged quantities fails: large underpredictions of wall and vapour temperatures are calculated, even when

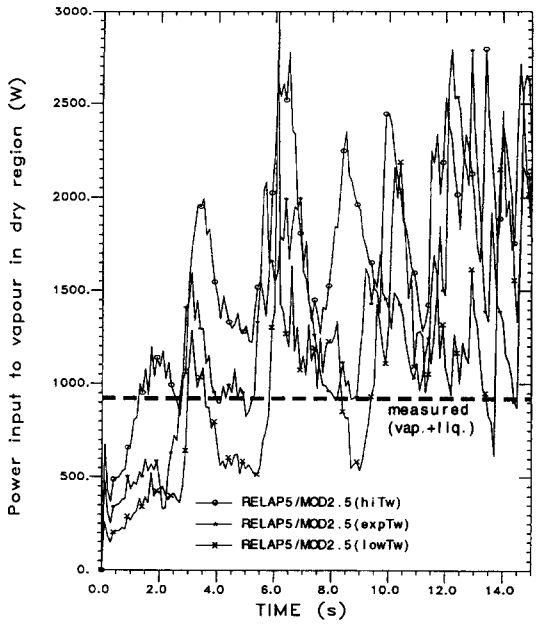

Fig. 21. Comparison of the heat transfer rate to the vapour calculated by RELAP5/MOD2.5 for various initial wall temperature distributions with the total power input measured in Test U351.

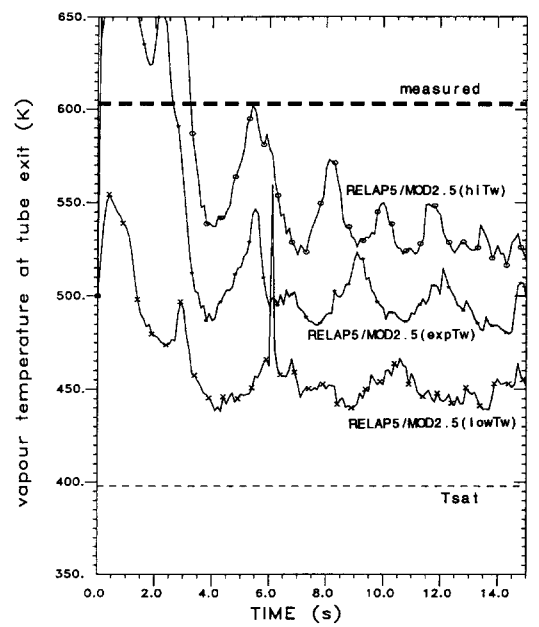

Fig. 22. Comparison of the calculated vapour temperature at the tube exit with the experimental value at the time of the mid-height quench in Test U351.

large values (4–5 mm) for the droplet diameter are used.

A map in the mass flux/void fraction plane has been generated, where two different regions of applicability of the 1-D models are clearly delineated. In the region of high mass fluxes or high void fractions, 1-D models can yield good results. For low mass fluxes and void fraction, however, no satisfactory results have been obtained by 1-D models (unless unphysically large values of the droplet diameter are used).

It has been thus concluded that, unless the classical closure laws for interfacial heat transfer and drag used in the present investigation are largely in error, the main deficiency of the 1-D approach consists in the overestimation of interfacial heat transfer. This is due to the use of the cross-sectionally averaged temperature difference between vapour and droplets, instead of the lower mean temperature of the vapour near the centre of the tube where the droplets actually reside.

The analysis of two tests (which required the need of 2-D treatment of the interfacial heat transfer) by means of two different 1-D codes, confirmed the intrinsic difficulties of the 1-D models of dispersed flow film boiling at low mass flux and low void fraction.

The consideration of 3-D droplet hydrodynamics within the frame of the present model yields a large accumulation of liquid in the central zone of the channel and this leads to substantial reductions of the interfacial heat transfer. Such a reduction is the key to the successful prediction of most of the thirty-two tests investigated, covering wide range of pressure, mass flux and quality conditions relevant to reflooding. Obviously, the 2-D effects proposed in the present work to explain the failure of the 1-D models are supported only by theoretical analyses and the confirmation of their existence can only be obtained by carefully designed experiments where the fine structure of the radial liquid distribution can be measured.

Several parametric studies have been performed to assess the validity of the above conclusions for various choices of the closure laws. The need to account for the evolution of the droplet spectrum was also challenged. It was recognized that, for most conditions, the choice of the correlations does not influence the main result: with a multidimensional approach, reasonably good agreement with the experimental results can be obtained, also for those conditions which were not amenable to 1-D analysis. It was also concluded that the correct estimation of the Sauter mean diameter and an adequate representation of the droplet spectrum are important, but the *details* of the evolution of the droplet population and of its equilibrium distribution play only a minor role. However, the use of a unique diameter for all the droplets may yield quite unrealistic results, as an 'average' droplet diameter is not capable of representing the different radial drifts of droplets having largely different sizes.

The prediction of interfacial heat transfer is strongly influenced by the Sauter mean diameter of the droplet population, becoming *larger* for larger Sauter mean diameter. As large droplets do exist above the quench front, inclusion of a capillary break-up mechanism is necessary to reduce their Sauter mean diameter further up under low mass flux conditions, when other break-up modes are not possible. The inclusion of

capillary break-up in the model is an effective way of circumventing the lack of information regarding the size of the droplets at their generation point. The break-up mechanism produces automatically the 'correct' Sauter mean diameter. However, the dependence of the good results on the presence of capillary break-up could be regarded as a weakness of the model. When a general correlation for the droplet diameter at the onset of dispersed flow film boiling becomes available, the resort to capillary break-up for obtaining small droplet diameters at the onset of dispersed flow film boiling for low mass flux conditions will probably not be necessary.

Because of the neglect of collision and coalescence phenomena, the peaking of the droplet radial distribution in the centre is certainly overestimated, so that the results obtained by the present model have to be considered as lower bounds for the interfacial heat transfer and upper (although realistic) bounds for the wall and vapour temperatures. However, no large errors are expected from this simplification, as the largest contribution to the reduction of the interfacial heat transfer (compared to the 1-D approach) comes from the absence of droplets in the high temperature region *close to the wall.*

REFERENCES

1. Andreani, M. and Yadigaroglu, G., A 3-D Eulerian–Lagrangian model of dispersed flow film boiling including a mechanistic description of the droplet spectrum evolution—I. The thermal–hydraulic model. *International Journal of Heat and Mass Transfer*, 1997, **40,** 1753–1772.
2. Andreani, M. and Yadigaroglu, G., Prediction methods for dispersed flow film boiling. *International Journal of Multiphase Flow*, 1994, **20** (Suppl.), 1–52.
3. Andreani, M., Studies of dispersed flow film boiling with 3-D Lagrangian hydrodynamics and a 2-D Eulerian vapour field. Ph.D. dissertation, Swiss Federal Institute of Technology, Zurich, Switzerland, 1992.
4. Seban, R. A., Grief, R., Yadigaroglu, G., Elias, E., Yu, K., Abdollahian, D. and Peak, W., UC-B reflood program: experimental data report. EPRI report NP-743, Electric Power Research Institute, Palo Alto, CA, 1978.
5. Seban, R. A., Reflooding of a vertical tube at 1, 2 and 3 Atmospheres. EPRI report NP-3191, Electric Power Research Institute, Palo Alto, CA, 1983.
6. Evans, D. G., Webb, S. W. and Chen, J. C., Measurement of axially varying non-equilibrium in post-critical-heat-flux boiling in a vertical tube. NUREG/CR-3363, Lehigh University, Bethlehem, PA, 1983.
7. Gottula, R. C., Condie, K. G., Sundaram, R. K., Neti, S., Chen, J. C. and Nelson, R., Forced convective, non-equilibrium, post-CHF heat transfer. Experiment data and correlation comparison report. NUREG/CR-3193, Idaho National Engineering Laboratories, Idaho Falls, ID, 1985.
8. Peake, W. T., Dispersed flow film boiling during reflooding. Ph.D. thesis, University of California, Berkeley, CA, 1979.
9. Kawaji, M., Transient non-equilibrium two-phase flow: reflooding of a vertical flow channel. Ph.D. thesis, University of California, Berkeley, CA, 1984.
10. Andreani, M. and Yadigaroglu, G., Parametric studies on droplet size distribution and break-up processes in dispersed flow film boiling during reflooding. In *Proceedings of the Sixth International Topical Meeting on Nuclear Reactor Thermal Hydraulics—NURETH* 6, Vol. 1. French Section of the American Nuclear Society, pp. 129–138.
11. Sarjeant, M., Drop break-up by gas streams. CGEB report R/M/N1005, Berkeley Nuclear Laboratories, London, 1978.
12. Pilch, M. and Erdman, C. A., Use of break-up time data and velocity history data to predict the maximum size of stable fragments for accelerations induced breakup of a liquid drop. *International Journal of Multiphase Flow*, 1986, **13,** 741–757.
13. Mugele, R. A. and Evans, H. D., Droplet size distribution in sprays. *Industrial & Engineering Chemistry*, 1951, **43,** 1317–1324.
14. Khan, H. J. and Kosaly, G., Subchannel void fraction analysis via drift-flux analysis. *Nuclear Technology*, 1986, **75,** 34–45.
15. Chexal, B. and Lellouche, G., A full range drift flux correlation for vertical flows. EPRI report NP-3989-SR, Electric Power Research Institute, Palo Alto, California, 1985.
16. Kocamustafaogullari, E., De Jarlais, G. and Ishii, M., Droplet generation during reflooding. *Transactions of the American Nuclear Society*, 1983, **45,** 804–805.
17. Ardron, K. H. and Hall, P. C., Droplet hydrodynamics and heat transfer in the dispersed flow regime in bottom reflooding. CEGB report RD/B/5007N81, Berkeley Nuclear Laboratories, London, 1981.
18. Renksizbulut, M. and Yuen, M. C., Experimental study of droplet evaporation in a high-temperature air stream. *Journal of Heat Transfer*, 1983, **105,** 384–388.
19. Ganic, E. N. and Rohsenow, W. M., On the mechanism of liquid drop deposition in two-phase dispersed flow. *Journal of Heat Transfer*, 1979, **101,** 288–294.
20. Lee, R. and Almenas, K., Droplet deposition above a quench front during reflooding. *Transactions of the American Nuclear Society*, 1982, **39,** 787–788.
21. Rubinow, S. I. and Keller, J. B., The transverse force on a spinning sphere in viscous fluid. *Journal of Fluid Mechanics*, 1961, **11,** 447–459.
22. Saffman, P. W., The lift on a small sphere in a slow shear flow. *Journal of Fluid Mechanics*, 1965, **22,** 385–400; also *Corrigendum*, 1968, **31,** 624.
23. Nelson, R. and Unal, C., A phenomenological model of the thermal hydraulics of convective boiling during the quenching of hot rod bundles. Part I: thermal hydraulic model. *Nuclear Engineering & Design*, 1992, **136,** 277–298.
24. Unal, C. and Nelson, R., A phenomenological model of the thermal hydraulics of convective boiling during the quenching of hot rod bundles. Part II: assessment of the model with steady-state and transient post-CHF data. *Nuclear Engineering & Design*, 1992, **136,** 299–318.
25. Unal, C. and Nelson, R., A phenomenological model of the thermal hydraulics of convective boiling during the quenching of hot rod bundles. Part III: assessment of the model using Winfrith steady-state, post-CHF, void fraction and heat transfer measurements and Berkeley transient reflood test data. *Nuclear Engineering & Design*, 1993, **140,** 211–227.
26. Andreani, M., Analytis, G. Th. and Aksan, N. S., On the model of interfacial heat transfer for the dispersed flow regime implemented in the RELAP5/MOD2.5 and RELAP5/MOD3 computer codes. Internal report TM-42-94-06, Paul Scherrer Institute, Villigen, Switzerland, 1994.